Molecular diffusion of stable water isotopes in polar firn as a proxy for past temperatures

C. Holme[1], V. Gkinis[1], and B. M. Vinther[1]

[1]The Niels Bohr Institute, Centre for Ice and Climate, Juliane Maries Vej 30, 2100 Copenhagen, Denmark

Abstract

Polar precipitation archived in ice caps contains information on past temperature conditions. Such information can be retrieved by measuring the water isotopic signals of δ^{18}O and δD in ice cores. These signals have been attenuated during densification due to molecular diffusion in the firn column, where the magnitude of the diffusion is isotopologoue specific and temperature dependent. By utilizing the differential diffusion signal, dual isotope measurements of δ^{18}O and δD enable multiple temperature reconstruction techniques. This study assesses how well six different methods can be used to reconstruct past surface temperatures from the diffusion-based temperature proxies. Two of the methods are based on the single diffusion lengths of δ^{18}O and δD, three of the methods employ the differential diffusion signal, while the last uses the ratio between the single diffusion lengths. All techniques are tested on synthetic data in order to evaluate their accuracy and precision. In addition, a benchmark test is applied to thirteen high resolution data sets from Greenland and Antarctica, which represent a broad range of mean annual surface temperatures and accumulation rates. The presented methods are found to accurately reconstruct the temperatures of the synthetic data, and the estimated temperatures are shown to be unbiased. Both the benchmark test and the synthetic data test demonstrate that the most precise reconstructions are obtained when using the single isotope diffusion lengths, with precisions around $0.5\,^\circ$C. In the benchmark test, the single isotope diffusion lengths are also found to reconstruct consistent temperatures with a root-mean-square-deviation of $0.7\,^\circ$C. The techniques employing the differential diffusion signals are more uncertain, where the most precise method has a precision of $1.5\,^\circ$C. The diffusion length ratio method is the least precise with a precision of $11.8\,^\circ$C. The absolute temperature estimates from this method are also shown to be highly sensitive to the choice of fractionation factor parameterization. From the combined analyses of the synthetic and ice core data, this study demonstrates that methods based on the single isotope diffusion lengths result in the most accurate and precise estimates of past temperatures.

Keywords

Holocene, paleoclimatology, ice cores, isotope geochemistry, stable isotopes, diffusion, Greenland, Antarctica.

1 Introduction

Polar precipitation stored for thousands of years at the ice caps of Greenland and Antarctica contains invaluable information on past climatic conditions. The isotopic composition of polar ice commonly expressed through the δ notation has been shown to work as a direct proxy of the relative depletion of a water vapor mass in its journey from the evaporation site to the place where condensation takes place (Epstein et al. 1951, Mook 2000). Additionally, for modern times, it shows a good correlation with the temperature of the cloud at the time of precipitation (Dansgaard 1954, 1964) and as a result it has been proposed and used as a proxy of past temperatures (Jouzel & Merlivat 1984, Jouzel et al. 1997, Johnsen et al. 2001).

The use of the isotopic paleothermometer presents however some notable limitations. The linear relationship between $\delta^{18}O$ and temperature commonly referred to as the "spatial slope" may hold for present conditions. However previous studies based on more physical principles as the borehole temperature reconstruction (Cuffey et al. 1994, Johnsen et al. 1995) as well as the thermal fractionation of the $\delta^{15}N$ signal in polar firn (Schwander et al. 1988, Severinghaus et al. 1998, Severinghaus & Brook 1999) have independently underlined the inaccuracy of the spatial isotope slope when it is extrapolated to past climatic conditions. Even though qualitatively the $\delta^{18}O$ signal comprises past temperature information, it fails to provide a quantitative picture on the magnitudes of past climatic changes.

In a seminal paper in 2000, Johnsen et al. (2000) set the foundations for the quantitative description of the diffusive processes the water isotopic signal undergoes in the porous firn layer from the time of deposition until pore close–off. Even though the main purpose of that work was to investigate how to reconstruct the part of the signal that was attenuated during the diffusive processes, the authors make a clear reference to the possibility of using the assessment of the diffusive rates as a proxy for past firn temperatures. The temperature reconstruction method based on isotope firn diffusion requires data of high resolution. More specifically, if one would like to look into the differential diffusion signal, datasets of both $\delta^{18}O$ and δD are required. Such data sets have until recently not been easy to obtain especially due to the challenging nature of the δD analysis (Bigeleisen et al. 1952, Vaughn et al. 1998). Nowadays, with the advent of commercial high–accuracy, high–precision Infra-Red spectrometers (Crosson 2008, Brand et al. 2009), simultaneous measurements of $\delta^{18}O$ and δD have become easier to obtain. Coupling of these instruments to Continuous Flow Analysis systems (Gkinis et al. 2011, Emanuelsson et al. 2015) can also result in measurements of ultra–high resolution, a necessary condition for accurate temperature reconstructions based on water isotope diffusion.

A number of existing works have presented past firn temperature reconstructions based on water isotope diffusion. Simonsen et al. (2011) and Gkinis et al. (2014) used high resolution isotopic datasets from the NorthGRIP ice core (members 2004). The first study makes use of the differential diffusion signal, utilizing spectral estimates of high–resolution dual δ^{18}O and δD datasets covering the GS–1 and GI–1 periods in the NorthGRIP ice core (Rasmussen et al. 2014). The second study presents a combined temperature and accumulation history of the past 16,000 years based on the power spectral density (**PSD** hereafter) signals of high resolution δ^{18}O measurements of the NorthGRIP ice core. More recently, van der Wel et al. (2015) introduced a slightly different approach for reconstructing the differential diffusion signal and testing it on dual δ^{18}O, δD high resolution data from the EDML ice core (Oerter et al. 2004). By artificially forward–diffusing the δD signal the authors estimate differential diffusion rates by maximizing the correlation between the δ^{18}O and δD signal.

In this work we attempt to look into all different flavors of temperature diffusion reconstruction techniques and assess their performance. We use synthetic, as well as real ice core data sets that represent Holocene conditions from a variety of drilling sites on Greenland and Antarctica. Our objective is to use data sections that originate from parts of the core as close to present day as possible. By doing this we aim to minimize possible uncertainties and biases in the ice flow thinning adjustment that is required for temperature interpretation of the diffusion rate estimates. Such a bias has been shown to exist for the NorthGRIP ice core (Gkinis et al. 2014), most likely due to the Dansgaard–Johnsen ice flow model overestimating the past accumulation rates for the site. For some cases however this was not possible and approximately half of the datasets used here have an age at approximately around Holocene Climate Optimum (**HCO** hereafter). Another interesting aspect of this study is that it uses water isotopic data sets of δ^{18}O and δD measured using different analytical techniques, namely Isotope Ratio Mass Spectroscopy (**IRMS** hereafter) as well as Cavity Ring Down Spectroscopy (**CRDS** hereafter). Two of the data sets presented here were obtained using Continuous Flow Analysis (**CFA** hereafter) systems tailored for water isotopic analysis (Gkinis et al. 2011). All data sections are characterized by a very high sampling resolution typically of $5\,\mathrm{cm}$ or better.

2 Diffusion of water isotope signals in firn

The main focus of this section is to outline the various temperature reconstruction techniques that can possibly be employed for paleotemperature reconstructions. The fundamentals of isotope diffusion theory are also presented. In order to avoid significant overlap with previously published works that have dealt with the matter e.g. Johnsen (1977), Johnsen et al. (2000), Simonsen et al. (2011), Gkinis et al. (2014), van der Wel et al. (2015) we occasionally point the reader to any of the latter or/and refer to specific sections in the Appendix. We exemplify and illustrate the use of various techniques using synthetic data prepared such that they resemble two representative regimes of ice coring sites on the Greenland summit and the East Antarctic Plateau.

The porous medium of the top $60-80\,\mathrm{m}$ of firn allows for a molecular diffusion process that attenuates the water isotope signal from the time of deposition until pore close–off. The process takes place in the vapor phase and it can be described by Fick's second law as:

$$\frac{\partial \delta}{\partial t} = D\left(t\right) \frac{\partial^2 \delta}{\partial z^2} - \dot{\varepsilon}_z\left(t\right) z\ \frac{\partial \delta}{\partial z} \tag{2.1}$$

where z is the depth from surface, δ refers to the water isotope ratio signal, $D\left(t\right)$ is the diffusivity coefficient and $\dot{\varepsilon}_z\left(t\right)$ the vertical strain rate. The attenuation of the isotopic signal results in loss of information. However the dependence of $\dot{\varepsilon}_z\left(t\right)$ and $D\left(t\right)$ on temperature and accumulation presents the possibility of using the process as a tool to infer these two paleoclimatic parameters. A solution to Eq. 2.1 can be given by the convolution of the initial isotopic profile δ' with a Gaussian filter $\mathcal{G}$ as:

$$\delta\left(z\right) = \mathcal{S}\left(z\right)\left[\delta'\left(z\right) * \mathcal{G}\left(z\right)\right] \tag{2.2}$$

where the Gaussian filter is described as:

$$\mathcal{G}\left(z\right) = \frac{1}{\sigma\sqrt{2\pi}}\, e^{\frac{-z^2}{2\sigma^2}} \quad , \tag{2.3}$$

and $\mathcal{S}$ is the total thinning of the layer at depth z described by

$$\mathcal{S}\left(z\right) = e^{\int_0^z \dot{\varepsilon}_z(z')\mathrm{d}z'} \quad . \tag{2.4}$$

In Eq. 2.3, the standard deviation term σ^2 represents the average displacement of a water molecule along the z–axis and is commonly referred to as the diffusion length. The σ^2 quantity is a direct measure of diffusion and its accurate estimate is critical to any attempt of reconstructing temperatures that are based on the isotope diffusion thermometer. Since it is directly related to the diffusivity coefficient and the strain rate -the latter for the case of the firn being approximately proportional to the densification rate-, it can be regarded as a sensor of firn temperature as well as accumulation rate.

The differential equation describing the evolution of σ^2 with time can be given by (Johnsen 1977):

$$\frac{\mathrm{d}\sigma^2}{\mathrm{d}t} - 2\,\dot{\varepsilon}_z(t)\,\sigma^2 = 2D(t) \quad . \tag{2.5}$$

In the case of firn the following approximation can be made for the strain rate:

$$\dot{\varepsilon}_z\left(t\right) \approx -\frac{\mathrm{d}\rho}{\mathrm{dt}}\,\frac{1}{\rho}. \tag{2.6}$$

Then we can solve Eq. 2.5 obtaining a solution for σ^2:

$$\sigma^2\left(\rho\right) = \frac{1}{\rho^2}\int_{\rho_o}^{\rho} 2\rho^2\left(\frac{\mathrm{d}\rho}{\mathrm{d}t}\right)^{-1} D(\rho)\;\mathrm{d}\rho, \tag{2.7}$$

where ρ_o is the surface density. Under the assumption that the diffusivity coefficient $D\left(\rho\right)$ and the densification rate $\frac{\mathrm{d}\rho}{\mathrm{d}t}$ are known, integration from surface density ρ_o to the close–off density ρ_{co} can be performed yielding a model based estimate for the diffusion length. In this work we make use of the Herron–Langway densification model (**H–L hereafter**) and the diffusivity rate parametrization introduced by Johnsen et al. (2000) (see Appendix A). Both $\frac{\mathrm{d}\rho}{\mathrm{d}t}$ and $D\left(\rho\right)$ are quantities that are dependent on both the temperature and the accumulation. This dependence of the diffusion length on temperature and accumulation provide the basis for the use of firn diffusion as a proxy of temperature and/or accumulation.

In Fig. 1 we evaluate Eq. 2.7 for all three isotopic ratios of water (δ^{18}O, δ^{17}O, δD) using boundary conditions characteristic of ice core sites from the Greenland and the Antarctic Ice Cap. For the first case we consider relatively warm and humid conditions (**WH** hereafter) representative of Greenlandic ice coring sites (e.g. GISP2, GRIP, NorthGRIP) with a surface temperature $T_{\mathrm{sur}} = -29\,^{\circ}\mathrm{C}$ and annual accumulation $A = 0.22\ \mathrm{myr}^{-1}\,\mathrm{w.eq}$. For the second case we consider relatively cold and dry conditions (**CD** hereafter) representative of Antarctic ice coring sites (e.g. Dome C, Vostok) with a surface temperature $T_{\mathrm{sur}} = -55\,^{\circ}\mathrm{C}$ and annual accumulation $A = 0.032\ \mathrm{myr}^{-1}\,\mathrm{w.eq}$.

3 Isotope diffusion in the solid phase

Below the close-off depth, diffusion occurs in solid ice driven by the isotopic gradients within the lattice of the ice crystals. This process is orders of magnitude slower than firn diffusion. Several studies exist that deal with the estimate of the diffusivity coefficient in ice (Blicks et al. 1966, Delibaltas et al. 1966, Itagaki 1964, Livingston et al. 1997, Ramseier 1967). The differences resulting from the various diffusivity coefficients are small and certainly negligible for the case of our study where the influence of solid ice diffusion is practically negligible. As done before by other similar firn diffusion studies (Johnsen et al. 2000, Simonsen et al. 2011, Gkinis et al. 2014) we make use of the parametrization given in Ramseier (1967) as:

$$D_{\mathrm{ice}} = 9.2\cdot 10^{-4}\cdot \exp\left(-\frac{7186}{T}\right)\mathrm{m^2s^{-1}}. \tag{3.1}$$

Assuming that a depth–age scale as well as a thinning function are available for the ice core a solution for the ice diffusion length is given by (see Appendix B for details):

$$\sigma^2_{\mathrm{ice}}(t') = S(t')^2\int_0^{t'} 2D_{\mathrm{ice}}(t)\,S(t)^{-2}\;\mathrm{d}t. \tag{3.2}$$

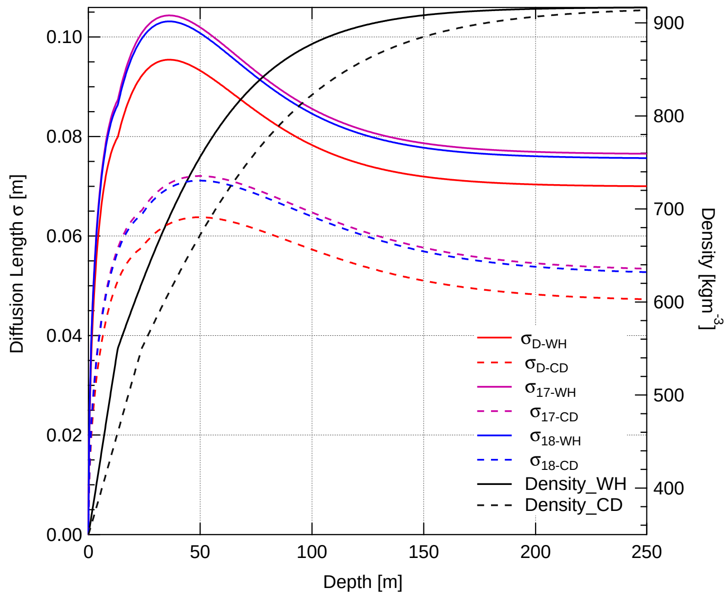

Figure 1: Diffusion length and density profiles for the WH (solid lines) and CD (dashed lines) scenarios for diffusion of the δ^{18}O (blue color), δ^{17}O (purple color) and δD (red color) isotope signals.

In Fig. 2 we have calculated ice diffusion lengths for four different cores (NGRIP, NEEM, Dome C, EDML). For the calculation of the diffusivities we have used high precision measurements of temperature borehole profiles and assumed a steady state condition. As it can be seen, for the low temperature/low accumulation sites of Dome C and EDML, σ_{ice} is lower. As the temperature of the ice increases closer to the bedrock σ_{ice} increases monotonically. For the special case of the Dome C core with a bottom age exceeding 800,000 years, σ_{ice} reaches values as high as 15 cm.

4 Reconstructing firn temperatures

4.1 The single isotopologue diffusion

The simplest implementation of the water isotope diffusion thermometer focuses on the assessment of the diffusion rates of one isotopologue in firn. Implementation of Eq. 2.7, yields diffusion length values from surface to close–off and below with ice thinning disregarded for now.

A fundamental property of the convolution operation is that it is equivalent to multiplication in the frequency domain. The transfer function of the diffusion process will be given by the Fourier transform of the Gaussian filter that will itself be a Gaussian function described by (Abramowitz & Stegun 1964,

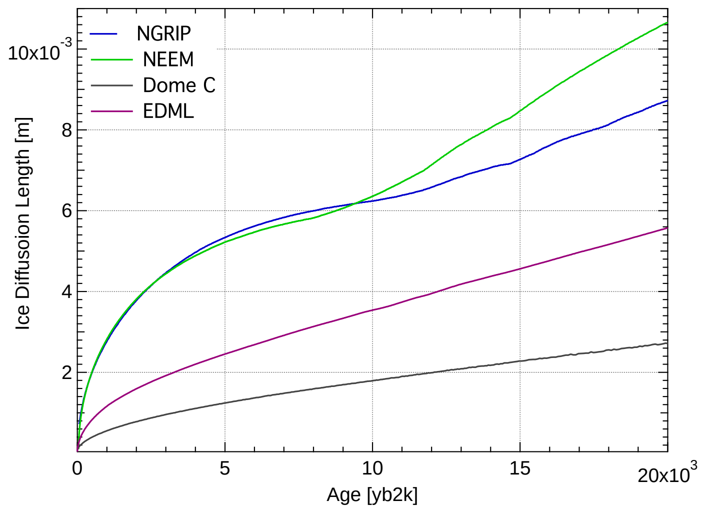

Figure 2: The ice diffusion length plotted with respect to age [b2k] for some selected sites from Greenland and Antarctica. NGRIP is represented by blue, NEEM is represented by green, Dome C is represented by grey and EDML is represented by magenta.

Gkinis et al. 2014):

$$\mathfrak{F}[\mathcal{G}(z)] = \hat{\mathcal{G}} = e^{\frac{-k^2\sigma^2}{2}} \quad . \tag{4.1}$$

In Eq. 4.1, $k = 2\pi/\Delta$ where Δ is the sampling resolution of the isotopic time series. In Fig. 3 we illustrate the effect of the diffusion transfer function on a range of wavelengths for $\sigma = 1,\ 2,\ 4 \text{ and } 8\ \mathrm{cm}$. Wavelengths in the order of $50\,\mathrm{cm}$ and above remain largely unaltered while signals with wavelengths shorter than $20\,\mathrm{cm}$ are heavily attenuated.

An estimate of the value of the diffusion length σ can be obtained by looking at the power spectrum of the diffused isotopic time series. Assuming a measurement noise signal $\eta\,(k)$ apparent in the time series a model describing the power spectrum is given by:

$$P_s = P_0 e^{-k^2\sigma^2} + |\hat{\eta}\,(k)\,|^2. \tag{4.2}$$

We find that the noise signal is generally described well by autoregression of order 1 (AR-1). The power spectral density of the latter may be written as (Kay & Marple 1981):

$$|\hat{\eta}(k)|^2 = \frac{\sigma_\eta^2 \Delta}{|1 + a_1 \exp\left(-ik\Delta\right)|^2}, \tag{4.3}$$

where a_1 is the AR-1 coefficient and σ_η^2 is the variance of the signal.

In Fig. 4 we show an example of power spectra based on a synthetic time series. The time series is generated using an AR-1 process with coefficient r_1 and variance ε

$$\delta_{\mathrm{n}} - r_1 \delta_{\mathrm{n}-1} = \varepsilon_{\mathrm{n}}. \tag{4.4}$$

The time series is subsequently diffused with a $8.2\,\mathrm{cm}$ diffusion length Gaussian filter and sampled discretely at $2.5\,\mathrm{cm}$ resolution. We also added measurement noise equal to $0.09‰$ (1 standard deviation). The spectral estimate of the time series $\mathbb{P}_s$ is calculated using Burg's spectral estimation method (Kay & Marple 1981) and specifically the algorithm presented in Andersen (1974). Using a least–squares approach we optimize the fit of P_s to $\mathbb{P}_s$ by varying the four parameters P_0, σ^2, a_1 and σ_η^2 The $|P_s - \mathbb{P}_s|^2$ least squares optimization resulted in a diffusion length of $8.5\,\mathrm{cm}$.

Assuming a diffusion length $\widehat{\sigma}_i^2$ is obtained for depth z_i by means of $|P_s - \mathbb{P}_s|^2$ minimization, one can calculate the equivalent diffusion length at the bottom of the firn column σ^2_{firn} in order to estimate firn temperatures by means of Eq. 2.7. In order to do this, one needs to take into account three necessary corrections. The first concerns the artifactually imposed diffusion due to the sampling of the ice core. In the case of a discrete sampling scheme with resolution Δ the additional diffusion length is (see Appendix C):

$$\sigma^2_{\mathrm{dis}} = \frac{2\Delta^2}{\pi^2} \ln\left(\frac{\pi}{2}\right) \tag{4.5}$$

In the case of high resolution measurements carried out with CFA measurement systems, there exist a number of ways to characterize the sampling diffusion length. Typically the step or impulse response of the CFA system can be measured yielding a Gaussian filter specific for the CFA system (Gkinis et al. 2011, Emanuelsson et al. 2015). The Gaussian filter can be characterized by a diffusion length σ^2_{cfa} that can be directly used to perform a sampling correction. The second correction concerns the ice diffusion as described in Sec. 3. The quantities σ^2_{ice} and σ^2_{dis} can be subtracted from $\widehat{\sigma}_i^2$ yielding a scaled value of σ^2_{firn} due to ice flow thinning. As a result, we can finally obtain σ^2_{firn} as:

$$\sigma^2_{\mathrm{firn}} = \frac{\widehat{\sigma}_i^2 - \sigma^2_{\mathrm{dis}} - \sigma^2_{\mathrm{ice}}}{\mathcal{S}(z)^2}. \tag{4.6}$$

When an estimate of σ^2_{firn} is obtained the integrated firn column temperature can be calculated by finding the roots of the equation:

$$\left(\frac{\rho_{co}}{\rho_i}\right)^2 \sigma^2(\rho = \rho_{\mathrm{co}}, T(z), A(z)) - \sigma^2_{\mathrm{firn}} = 0 \tag{4.7}$$

where σ^2 is the result of the integration in Eq. 2.7 from surface to close–off density ($\rho_o \to \rho_{\mathrm{co}}$). In this work we use a Newton-Raphson numerical scheme (Press et al. 2007) for the calculation of the roots of the equation.

As it can be seen, the accuracy of the σ^2_{firn} estimation and subsequently of the temperature reconstruction obtained based on it, depends on the three correction terms σ^2_{ice}, σ^2_{dis} and the ice flow thinning $\mathcal{S}(z)$. For relatively shallow depths where σ^2_{ice} is relatively small compared to $\widehat{\sigma}_i^2$, ice diffusion can be accounted for with simple assumptions on the borehole temperature profile and the ice flow. In a similar way, σ^2_{dis} is a well constrained parameter and depends only on the sampling resolution Δ for discrete sampling schemes or the smoothing of the CFA measurement system.

Equation 4.6 reveals an interesting property of the single isotopologue temperature estimation technique. As seen, the result of the σ^2_{firn} calculation depends strongly on the ice flow thinning quantity $\mathcal{S}(z)^2$. Possible errors in the estimation of $\mathcal{S}(z)^2$ due to imperfections in the modelling of the ice flow will inevitably be propagated to the σ^2_{firn} value thus biasing the temperature estimation. Even though this appears to be a disadvantage in the method, it can be a useful tool for assessing the accuracy of ice flow models. Provided that for certain sections of the ice core there is a temperature estimate available based on other reconstruction methods (borehole thermometry, $\delta^{15}\text{N}/\ \delta^{40}\text{Ar}$) it is possible to estimate ice flow induced thinning of the ice core layers. Following this approach Gkinis et al. (2014) proposed a correction in the existing accumulation rate history for the NorthGRIP ice core.

The annual spectral signal interference

For some of the processed ice core data, we observed a prominent spectral feature at the low frequency area coinciding with the annual water isotopic signal. These spectral features are more likely to manifest in ice cores with boundary conditions that mitigate the effects of firn diffusion, notably low temperatures and high accumulation rates. The resulting effect of such a spectral signature, is the artifactual biasing of the diffusion length estimation towards lower values and thus colder temperatures. Figure 5 shows the PSD of the δD series for a mid Holocene section from the GRIP ice core (drill site characteristics in Table II). A prominent spectral feature is visible at $f \approx 6\,\text{cycles}\,\text{m}^{-1}$. This frequency is comparable to the expected frequency of the annual signal at $6.1\,\text{cycles}\,\text{m}^{-1}$ as estimated from the annual layer thickness reconstruction of the GICC05 timescale (Vinther et al. 2006).

In order to evade the influence of the annual spectral signal on the diffusion length estimation, we propose the use of a weight function $w(f)$ in the spectrum as:

$$w(f) = \begin{cases} 0 & f_\lambda - \mathrm{d}f_\lambda \le f \le f_\lambda + \mathrm{d}f_\lambda \\ 1 & f < f_\lambda - \mathrm{d}f_\lambda, f > f_\lambda + \mathrm{d}f_\lambda \end{cases} \tag{4.8}$$

where f_λ is the frequency of the annual layer signal based on the reconstructed annual layer thickness λ and $\mathrm{d}f_\lambda$ is the range around the frequency f_λ at which the annual signal is detectable. The weight function is multiplied with the optimization norm $|P_s - \mathbb{P}_s|^2$. Figure 5 also illustrates the effect of the

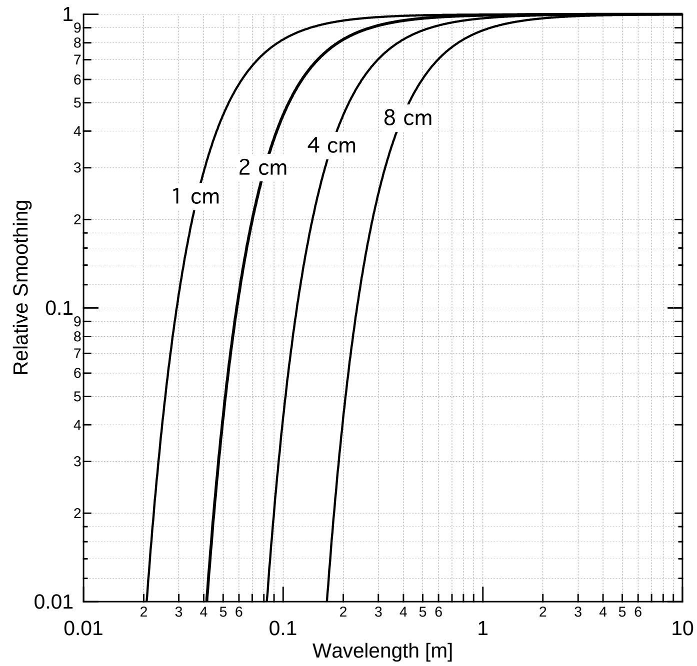

Figure 3: The smoothing effect of the diffusion transfer function demonstrated on a range of different wavelengths for $\sigma = 1,\, 2,\, 4$ and 8 cm.

weight function on the estimation of P_s and subsequently the diffusion length value. When the weight function is used during the optimization process, there is an increase in the diffusion length value by 0.2 cm, owing essentially to the exclusion of the annual signal peak from the minimization of $|P_s - \mathbb{P}_s|^2$. While the value of f_λ can be roughly predicted the value of $\mathrm{d}f_\lambda$ usually requires visual inspection of the spectrum. Annual peak corrections are included in the study of the ice core time series introduced in Sec. 5.2.

4.2 The differential diffusion signal

A second-order temperature reconstruction technique is possible based on the differential signal between δ^{18}O and δD. Due to the difference in the fractionation factors and the air diffusivities between the oxygen and deuterium isotopologues, a differential diffusion signal is created in the firn column. Based on the calculation of the diffusion lengths presented in Fig. 1 we then compute the differential diffusion lengths $^{17}\Delta\sigma^2$ and $^{18}\Delta\sigma^2$ where

$$^{17}\Delta\sigma^2 = \sigma_{17}^2 - \sigma_{\mathrm{D}}^2 \;\text{ and }\; ^{18}\Delta\sigma^2 = \sigma_{18}^2 - \sigma_{\mathrm{D}}^2. \tag{4.9}$$

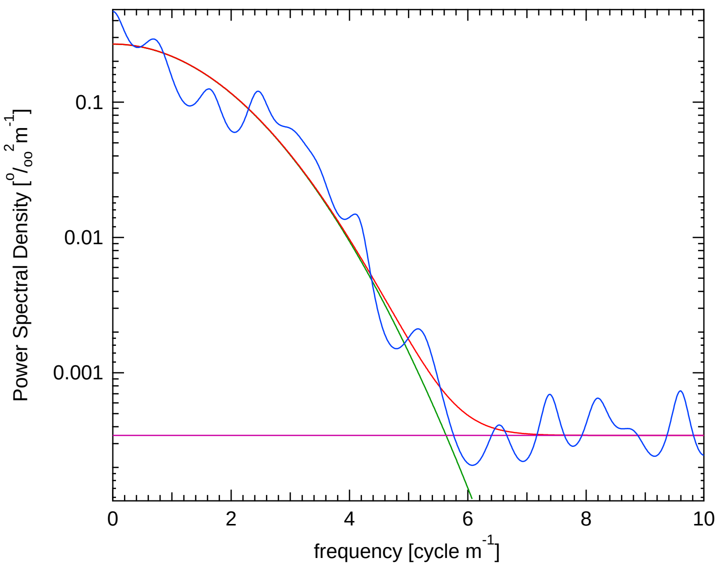

Figure 4: PSD of a synthetic δ^{18}O time series plotted with respect to frequency (blue curve), the red curve represents the complete model fit (Eq. 4.2), the green curve represents the signal part of the fit and the magenta curve represents the noise part of the fit.

As it can be seen in Fig. 6 the differential diffusion length signal is stronger for the case of $^{17}\Delta\sigma^2$ when compared to $^{18}\Delta\sigma^2$.

One obvious complication of the differential diffusion technique is the requirement for dual measurements of the water isotopologues, preferably performed on the same sample. The evolution of IRMS techniques targeting the analysis of δD (Bigeleisen et al. 1952, Vaughn et al. 1998, Gehre et al. 1996, Begley & Scrimgeour 1997) in ice cores has allowed for dual isotopic records at high resolutions. With the advent of CRDS techniques and their customisation for CFA measurements, simultaneous high resolution measurements of both δ^{18}O and δD have become a routine procedure.

The case of δ^{17}O is more complicated as the greater abundance of ^{13}C than ^{17}O rules out the possibility for an IRMS measurement at mass/charge ratio (m/z) of 45 or 29 using CO_2 equilibration or reduction to CO respectively. Alternative approaches that exist include the electrolysis method with $CuSO_4$ developed by Meijer & Li (1998) as well as the fluorination method presented by Baker et al. (2002) and implemented by Barkan & Luz (2005) for dual-inlet IRMS systems. These techniques target the measurement of the $^{17}O_{excess}$ parameter and are inferior for δ^{17}O measurements at high precision and have a very low sample throughput. As a result, high resolution δ^{17}O measurements from ice cores are currently non existent. Recent innovations however in CRDS spectroscopy (Steig et al. 2014) allow for simultaneous triple

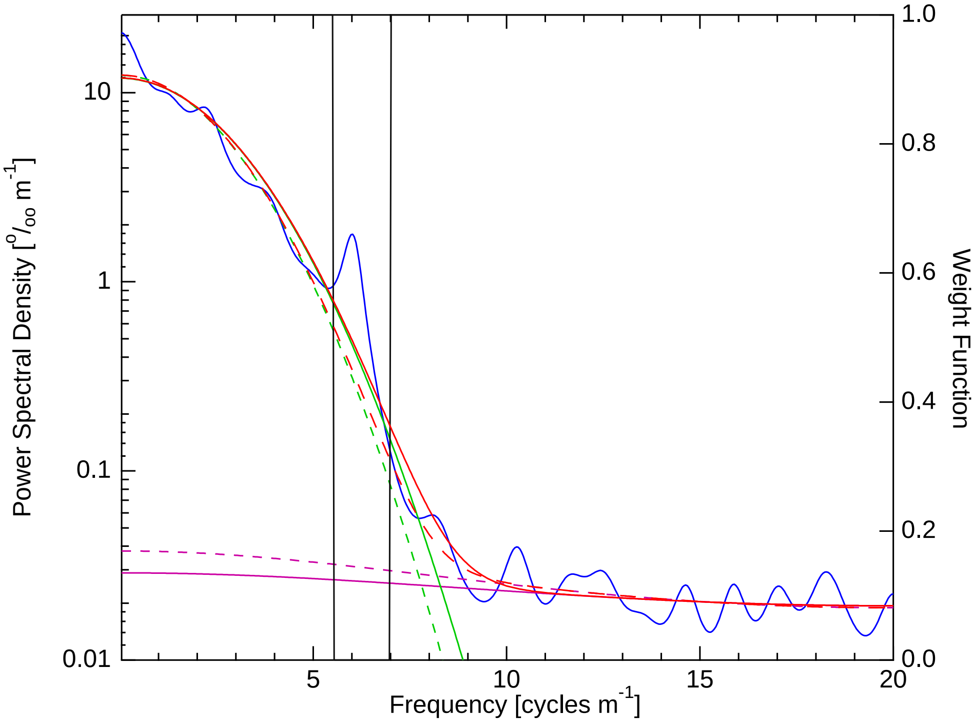

Figure 5: The interference of the annual spectral signal is seen in the PSD of the δD GRIP mid Holocene section. The regular fit is represented by the solid lines and the dashed lines represent the case where the weight function $w(f)$ has filtered out this artifactual bias.

isotopic measurements of δD, δ^{18}O and δ^{17}O in a way that a precise and accurate measurement for both δ^{17}O and ^{17}O$_{\mathrm{excess}}$ is possible. Therefore high resolution ice core datasets of δD, δ^{18}O and δ^{17}O should be expected in the near future.

The following analysis is focused on the $^{18}\Delta\sigma^2$ signal but it applies equally to the $^{17}\Delta\sigma^2$. The stronger attenuation of the δ^{18}O signal with respect to the δD signal can be visually observed in the power spectral densities of the two signals. As seen in Fig. 7 the $\mathbb{P}_{\mathrm{S18}}$ signal reaches the noise level at a lower frequency when compared to the $\mathbb{P}_{\mathrm{SD}}$ signal. At low frequencies with high signal to noise ratio we can calculate the logarithm of the ratio of the two power spectral densities as:

$$\ln\left(\frac{P_{\mathrm{D}}}{P_{18}}\right) \approx k^2\left(\sigma_{18}^2 - \sigma_{\mathrm{D}}^2\right) + \ln\left(\frac{P_{0_{\mathrm{D}}}}{P_{0_{18}}}\right) = {}^{18}\Delta\sigma^2\, k^2 + C, \tag{4.10}$$

As seen in Eq. 4.10 and Fig. 7 (δ^{18}O and δD synthetic data generated as in section 4.1) an estimate of the $^{18}\Delta\sigma^2$ parameter can be obtained by a linear fit of $\ln(P_{\mathrm{D}}/P_{18})$ in the low frequency area, thus requiring only two parameters ($^{18}\Delta\sigma^2$ and C) to be tuned. An interesting aspect of the differential diffusion method, is that in contrast to the single isotopologue diffusion length, ${}^{18}\Delta\sigma^2_{\mathrm{firn}}$ is a quantity that is independent of the sampling and solid ice diffusion thus eliminating the uncertainties associated with these two parameters. This can be seen by simply using Eq. 4.6:

$$ {}^{18}\Delta\sigma^2_{\mathrm{firn}} = \frac{\hat{\sigma}^2_{18} - \sigma^2_{\mathrm{dis}} - \sigma^2_{\mathrm{ice}}}{\mathcal{S}(z)^2} - \frac{\hat{\sigma}^2_{\mathrm{D}} - \sigma^2_{\mathrm{dis}} - \sigma^2_{\mathrm{ice}}}{\mathcal{S}(z)^2} = \frac{\hat{\sigma}^2_{18} - \hat{\sigma}^2_{\mathrm{D}}}{\mathcal{S}(z)^2} \tag{4.11} $$

Accurate estimates of the thinning function however play a key role in the differential diffusion technique.

One more complication of the differential diffusion technique is the selection of the frequency range in which one chooses to apply the linear regression. Often visual inspection is required in order to designate a cut-off frequency until which the linear regression can be applied. In most cases identifying the cut-off frequency, or at least a reasonable area around it is reasonably straight-forward though in a small number of case spectral features in the low frequency area seem to have a strong influence on the slope of the linear regression and thus on the ${}^{18}\Delta\sigma^2$. As a result, visual inspection of the regression result is always advised in order to avoid biases.

Another way of estimating the differential diffusion signal is to subtract the single diffusion spectral estimates σ^2_{18} and σ^2_{D}. Theoretically this approach should be inferior to the linear fit approach due to the fact that more degrees of freedom are involved in the estimation of σ^2_{18} and σ^2_{D} (8 versus 2). Here we will test both approaches.

Linear correlation method

An alternative way to calculate the differential diffusion signal ${}^{18}\Delta\sigma^2$, can be based on the assumption that the initial precipitated isotopic signal presents a $\mathrm{D_{xs}}$ that is invariable with time and as a consequence of this, the correlation signal $\rho_{\delta^{18}\mathrm{O}/\delta\mathrm{D}}$ is expected to have a maximum value at the time of deposition. From the moment of deposition, preferential diffusion of the δ^{18}O with respect to the δD, signal results in a decrease of the $\rho_{\delta^{18}\mathrm{O}/\delta\mathrm{D}}$ value, such that forward diffusing the δD signal with a Gaussian kernel of standard deviation equal to ${}^{18}\Delta\sigma^2$ will maximize the value of $\rho_{\delta^{18}\mathrm{O}/\delta\mathrm{D}}$ (van der Wel et al. 2015).

This type of estimation is independent of spectral estimates of the δ^{18}O and δD time series and does not pose any requirements for measurement noise characterization or selection of cut-off frequencies. However uncertainties related to the densification and ice flow processes, affect this method equally as they do for the spectrally based differential diffusion temperature estimation. In this study, we test the applicability of the method on synthetic and real ice core data, acknowledging that the assumption that the $\mathrm{D_{xs}}$ signal is constant with time is most likely false -something that certainly applies on millennial time scales- and is thus likely to result in inaccuracies.

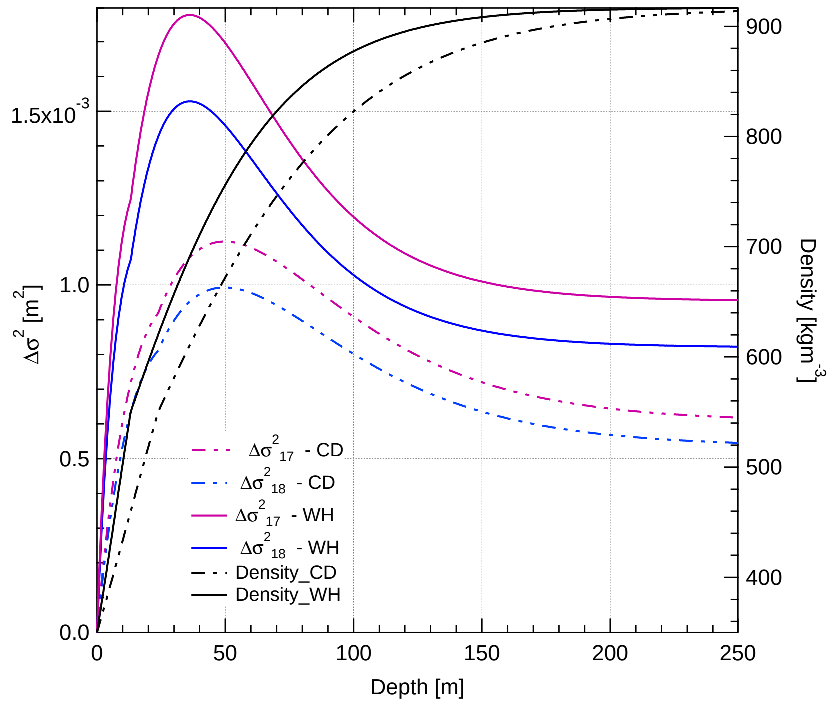

Figure 6: Differential diffusion lengths for the WH (solid lines) and CD (dashed lines) scenarios for $^{18}\Delta\sigma^2$ (blue) and $^{17}\Delta\sigma^2$ (purple). The density profiles are represented with black.

4.3 The diffusion length ratio

A third way of using the diffusion lengths as proxies for temperature can be based on the calculation of the ratio of two different diffusion lengths. From Eq. 2.7 we can evaluate the ratio of two different isotopologues j and k as:

$$\frac{\sigma_j^2(\rho)}{\sigma_k^2(\rho)} = \frac{\dfrac{1}{\rho^2}\displaystyle\int 2\rho^2\left(\frac{\mathrm{d}\rho}{\mathrm{d}t}\right)^{-1} D_j(\rho)\,\mathrm{d}\rho}{\dfrac{1}{\rho^2}\displaystyle\int 2\rho^2\left(\frac{\mathrm{d}\rho}{\mathrm{d}t}\right)^{-1} D_k(\rho)\,\mathrm{d}\rho}, \tag{4.12}$$

and by substituting the firn diffusivities as defined in Appendix A and according to Johnsen et al. (2000) we get:

$$\frac{\sigma_j^2(\rho)}{\sigma_k^2(\rho)} = \frac{D_{\mathrm{a}j}\alpha_k}{D_{\mathrm{a}k}\alpha_j}\,\frac{\dfrac{1}{\rho^2}\displaystyle\int 2\rho^2\left(\frac{\mathrm{d}\rho}{\mathrm{d}t}\right)^{-1}\frac{m\,p}{R\,T\,\tau}\left(\frac{1}{\rho}-\frac{1}{\rho_{\mathrm{ice}}}\right)\mathrm{d}\rho}{\dfrac{1}{\rho^2}\displaystyle\int 2\rho^2\left(\frac{\mathrm{d}\rho}{\mathrm{d}t}\right)^{-1}\frac{m\,p}{R\,T\tau}\left(\frac{1}{\rho}-\frac{1}{\rho_{\mathrm{ice}}}\right)\mathrm{d}\rho} = \frac{D_{\mathrm{a}j}\alpha_k}{D_{\mathrm{a}k}\alpha_j}. \tag{4.13}$$

As a result, the ratio of the diffusion lengths is dependent on temperature through the parameterizations of the fractionation factors and carries no dependence to parameters related to the densification rates

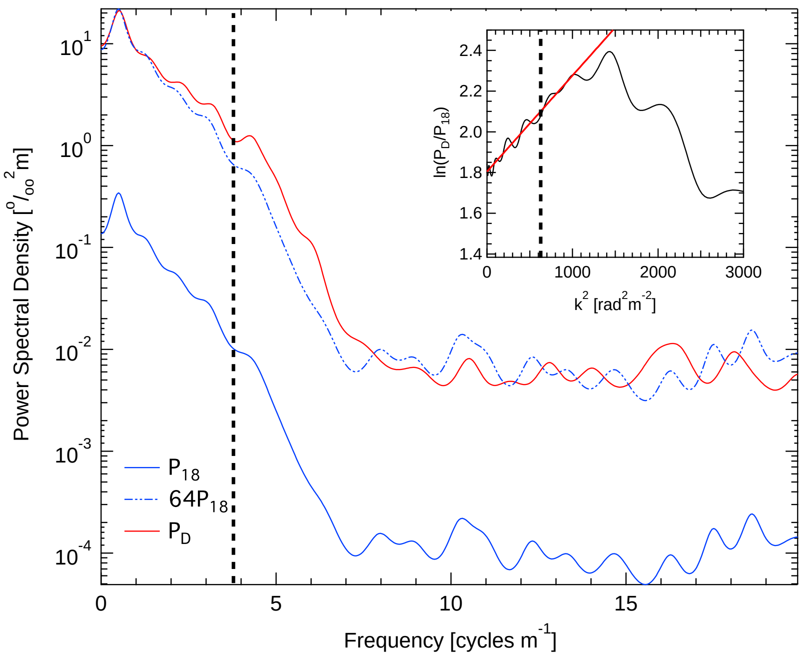

Figure 7: PSDs of δ^{18}O (blue) and δD (red) with respect to frequency where the inner subplot shows the $\ln(P_{\mathrm{D}}/P_{18})$ relation with respect to k^2. The ${}^{18}\Delta\sigma^2$ value is determined from the slope of the linear fit. The chosen cutoff frequency is marked by the vertical dashed line in the main plot.

nor the atmospheric pressure. Additionally, it is a quantity that is independent of depth. Here we give the analytical expressions of all the isotopologues combinations by substituting the diffusivities and the fractionation factors:

$$\sigma_{18}^2/\sigma_{\mathrm{D}}^2 = 0.93274 \cdot \exp(16288/T^2 - 11.839/T) \tag{4.14}$$

$$\sigma_{17}^2/\sigma_{\mathrm{D}}^2 = 0.933 \cdot \exp(16288/T^2 - 6.263/T) \tag{4.15}$$

$$\sigma_{18}^2/\sigma_{17}^2 = 0.99974 \cdot \exp(-5.57617/T) \tag{4.16}$$

A data-based diffusion length ratio estimate can be obtained by estimating the single diffusion length values as described in Sec. 4.1 and thereafter applying the necessary corrections as in Eq. 4.6. An interesting aspect of the ratio estimation is that it is not dependent on the ice flow thinning as seen below:

$$\left(\frac{\sigma_{18}^2}{\sigma_{\mathrm{D}}^2}\right)_{\mathrm{firn}} = \frac{\hat{\sigma}_{18}^2 - \sigma_{\mathrm{dis}}^2 - \sigma_{\mathrm{ice}}^2}{\hat{\sigma}_{\mathrm{D}}^2 - \sigma_{\mathrm{dis}}^2 - \sigma_{\mathrm{ice}}^2}. \tag{4.17}$$

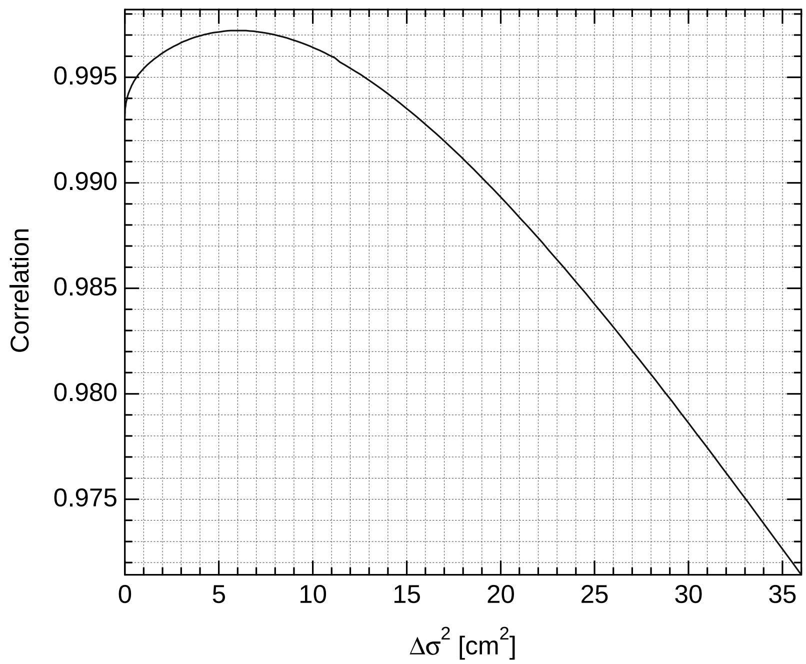

Figure 8: Correlation coefficient between the δ^{18}O and the forward–diffused δD series as a function of $^{18}\Delta\sigma^2$. The synthetic data have been generated to simulated a CD scenario as in Sec. 4.1

5 Results

5.1 Synthetic data test

We present here a test of accuracy and precision for the estimates of the various quantities used for diffusion based temperature estimations. The tests consist of the generation of synthetic data for δ^{17}O, δ^{18}O and δD and subsequent numerical diffusion with diffusion lengths as calculated for the WH and CD boundary conditions and presented in Fig. 1. The time series are then sampled at a certain resolution Δ and measurement noise is added. Eventually, estimates of diffusion lengths for all three isotopologues are obtained using the techniques we have described in the previous sections.

We start with the generation of δ^{18}O synthetic time series using the method outlined in Sec. 4.1. For the AR-1 process we use $r_1 = 0.3$ and $\varepsilon = 120\,‰^2$ for CD and $200\,‰^2$ for WH. The data section is $20\,\mathrm{m}$ long and has an initial spacing of $10^{-3}\,\mathrm{m}$. The δD and δ^{17}O series are then generated assuming a $\mathrm{D_{xs}}$ signal of $10\,‰$ and an Δ^{17}O signal of 0 per meg:

$$\delta\mathrm{D} = 8 \cdot \delta^{18}\mathrm{O} + 10‰ \tag{5.1}$$

$$\Delta^{17}\mathrm{O} = \ln(\delta^{17}\mathrm{O} + 1) - 0.528\ln(\delta^{18}\mathrm{O} + 1) \tag{5.2}$$

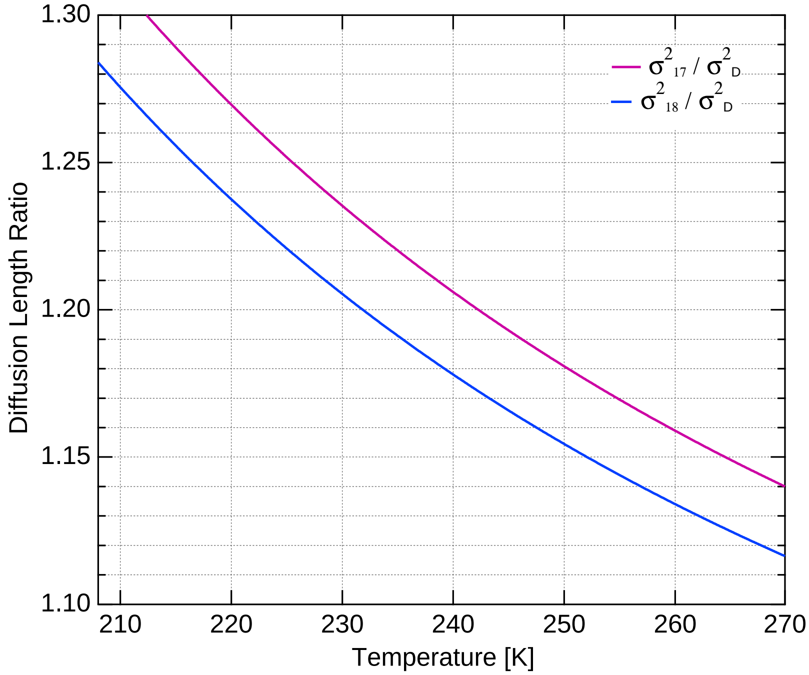

Figure 9: The diffusion length ratios $\sigma^2_{18}/\sigma^2_{\mathrm{D}}$ and $\sigma^2_{17}/\sigma^2_{\mathrm{D}}$ with respect to temperature. The $\sigma^2_{18}/\sigma^2_{17}$ is omitted due to its very low temperature sensitivity.

The isotopic series are then forward-diffused by means of numerical convolution with a Gaussian filter of variance σ^2 equal to the diffusion length for every case (Table I). Sampling with a discrete scheme of $\Delta = 0.025\,\mathrm{m}$ and addition of white measurement noise completes the process of the time series generation. We use 0.05, 0.07 and $0.5\,‰$ for δ^{17}O, δ^{18}O and δD respectively, with the numbers being representative of measurements uncertainties we have been observing over years of ice core measurements in our laboratory. We repeat the process of time series generation 500 times. For each iteration we estimate the quantities σ_{17}, σ_{18}, σ_{D}, $^{17}\Delta\sigma^2$, $^{18}\Delta\sigma^2$ and the ratios $\sigma^2_{18}/\sigma^2_{\mathrm{D}}$, $\sigma^2_{17}/\sigma^2_{\mathrm{D}}$ and $\sigma^2_{18}/\sigma^2_{17}$. The differential diffusion signals are estimated using the three different techniques as described in Sec. 4.2. We designate the subtraction technique with I, the linear regression with II and the correlation method with III. For every value of the diffusion estimates we calculate a firn temperature. Finally for the total of the 500 iterations we calculate a mean firn temperature $\overline{T}_{\text{firn}}$, a standard deviation $\sigma_{\overline{T}}$ and a mean bias as:

$$\mathrm{MB} = \frac{1}{N}\sum_{i=1}^{N} T_i - T_{\text{sur}} = \overline{T}_{\text{firn}} - T_{\text{sur}}, \tag{5.3}$$

where $i = 1, 2, \ldots, N$ signifies the iteration number, T_i is the synthetic data-based estimated temperature and T_{sur} is the model forcing surface temperature for the WH and CD scenarios. The results of the

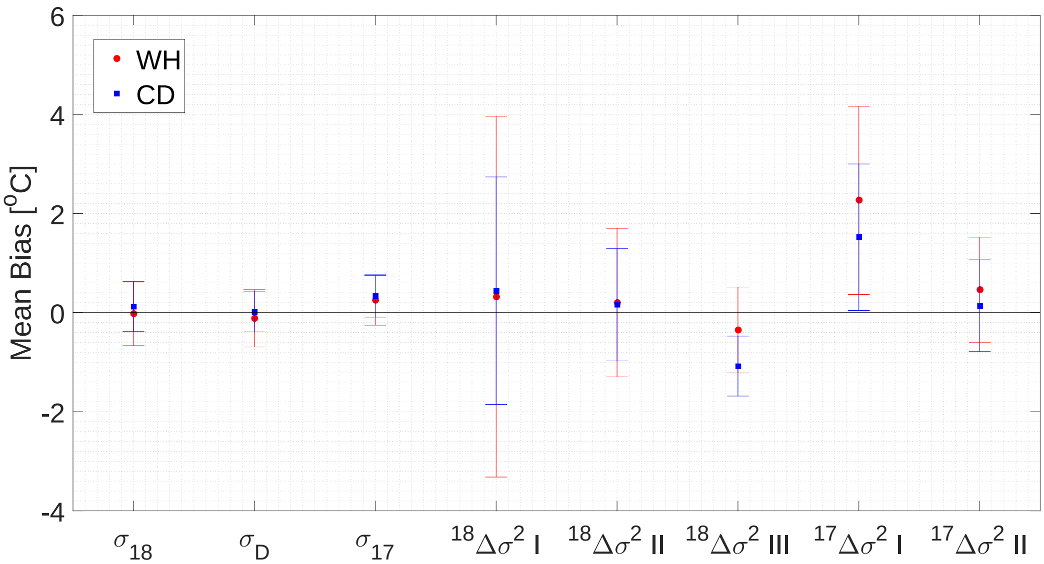

Figure 10: Mean biases for the single and differential diffusion. The error bars represent $1\sigma_{\bar{T}}$

experiment are presented in Table I and the calculated mean biases are illustrated in Fig. 10. The diffusion length ratio approach presents very large uncertainty bars and thus these results are not included in Fig. 10.

5.2 Ice core data test

We also use a number of high resolution, high precision ice core data, in order to benchmark the diffusion temperature reconstruction techniques that we have presented. The aim of this benchmark test is to utilize the various reconstruction techniques for a range of boundary conditions that is (a) as broad as possible with respect to mean annual surface temperature and accumulation and (b) representative of existing polar ice core sites. Additionally, we have made an effort in focusing on ice core data sets that reflect conditions as close as possible to present. As a result, the majority of the data sets presented here are from relatively shallow depths and as a result reflect climatic conditions typical of the late Holocene. Where this was not possible due to limited data availability, we have used data originating from deeper sections of the ice cores with an age of about 10ka b2k reflecting conditions of the early Holocene. In Table II we provide relevant information for each data set as well as the present temperature and accumulation conditions for the drill site from which each data set originates.

The data sets were produced using a variety of techniques both with respect to the analysis itself

	CD			WH		
	Input diffusion	Output diffusion	Est. T [^{o}C]	Input diffusion	Output diffusion	Est. T [^{o}C]
σ_{18}	5.73 cm	5.81 ± 0.13 cm	-54.9 ± 0.5	8.40 cm	8.43 ± 0.20 cm	-29.0 ± 0.6
σ_{D}	5.13 cm	5.20 ± 0.10 cm	-55.0 ± 0.4	7.77 cm	7.78 ± 0.20 cm	-29.1 ± 0.6
σ_{17}	5.80 cm	5.94 ± 0.12 cm	-54.7 ± 0.4	8.50 cm	8.61 ± 0.16 cm	-28.8 ± 0.5
$^{18}\Delta\sigma^2$ I	6.5 cm^2	6.8 ± 1.3 cm^2	-54.6 ± 2.3	10.2 cm^2	10.6 ± 2.2 cm^2	-28.7 ± 3.6
$^{18}\Delta\sigma^2$ II	6.5 cm^2	6.5 ± 0.6 cm^2	-54.8 ± 1.1	10.2 cm^2	10.3 ± 0.9 cm^2	-28.7 ± 1.2
$^{18}\Delta\sigma^2$ III	6.5 cm^2	5.9 ± 0.3 cm^2	-56.0 ± 0.5	10.2 cm^2	10.0 ± 0.5 cm^2	-29.4 ± 0.9
$^{17}\Delta\sigma^2$ I	7.3 cm^2	8.3 ± 1.2 cm^2	-53.5 ± 1.5	11.9 cm^2	13.6 ± 1.6 cm^2	-26.7 ± 1.9
$^{17}\Delta\sigma^2$ II	7.3 cm^2	7.4 ± 0.6 cm^2	-54.9 ± 0.9	11.9 cm^2	12.2 ± 0.8 cm^2	-28.5 ± 1.1
$\sigma_{18}^2/\sigma_{17}^2$	0.975	0.957 ± 0.040	————	0.977*	0.959 ± 0.027*	————
$\sigma_{18}^2/\sigma_{\mathrm{D}}^2$	1.24	1.25 ± 0.05	-56.9 ± 12.9	1.17	1.18 ± 0.04	-30.7 ± 16.0
$\sigma_{17}^2/\sigma_{\mathrm{D}}^2$	1.28	1.31 ± 0.05	-63.4 ± 8.9	1.20	1.23 ± 0.03	-40.0 ± 9.9

Table I: Simulations of a synthetic CD and WH scenario. The mean values and standard deviations of the output diffusion lengths are shown together with the corresponding temperatures.

(IRMS/CRDS), as well as with respect to the sample resolution and preparation (discrete/CFA). The majority of the data sets was analysed using CRDS instrumentation. In particular the L1102i, L2120i and L2130i variants of the picarro CRDS analyser were utilized for both discrete and CFA measurements of δ^{18}O and δD. The rest of the data sets were analysed using IRMS techniques with either $\mathrm{CO_2}$ equilibration or high temperature carbon reduction. For the case of the NEEM early Holocene data set, we work with two data sections that span the same depth interval and consist of discretely sampled and CFA measured data respectively. Additionally, the Dome C and Dome F data sections represent conditions typical for the East Antarctic Plateau and are sampled using a different approach ($2.5\,\mathrm{cm}$ resolution discrete samples for the Dome C section and high resolution CFA measurements for the Dome F section).

In a way similar to the synthetic data test, we apply the various reconstruction techniques on every ice core data section, we estimate the corresponding diffusion parameters and subsequently the temperatures corresponding to them. No reconstruction techniques involving δ^{17}O are presented here due to the lack of δ^{17}O data. In order to achieve an uncertainty estimation for every reconstruction, we perform a sensitivity test that is based on 1000 repetitions. Assuming that every ice core section consists of J δ^{18}O and δD points, then a repetition is based on a data subsection with size J' that varies in the interval $[J/2, J]$. This "jittering" of the subsection size happens around the midpoint of every section and J' is drawn from a uniform distribution. Eventually, for every reconstruction method and every ice core site, we calculate a mean and a standard deviation for the diffusion estimate, as well as a mean and a standard deviation for the temperature (T_{sur}, $\sigma_{\bar{T}}$). We would like to point out that this type of sensitivity test does not take into account uncertainties originating from the densification or diffusion physical quantities and their parameterizations, or inaccuracies due to the ice flow thinning model or solid ice and sampling diffusion estimates. Results are presented in Table III. The estimated temperatures for ice cores covering the late and early Holocene are shown in Fig. 11 and 12 respectively.

5.3 The fractionation factors

The influence of the fractionation factors (α_{18}, α_{D}) on the reconstructed temperatures are tested on ice core data sets representative of a broad range of temperatures. By comparing the results of different parameterization schemes, it is possible to quantify the influence of the choice of parametrization on the absolute temperature estimates. This is especially relevant for temperatures below -40°C, as the confidence of the parameterized fractionation factors have been shown to be low for such cold temperatures (Ellehoj et al. 2013). Similar to the ice core data test (Sec. 5.2), the corresponding diffusion parameters and subsequently the temperatures are based on a sensitivity test of 1000 repetitions. The results are displayed in Fig. 13, where the temperatures resulting from the parametrizations of Majoube (1970) (α_{18}) and Merlivat & Nief (1967) (α_{D}) are compared to the temperatures resulting from the parametrizations of Ellehoj et al. (2013) (α_{18}, α_{D}) and Lamb et al. (2015) (α_{D}). In the latter case, the parameterization of α_{18} from Majoube (1970) is used for the dual diffusion length methods.

6 Discussion

6.1 Synthetic data

Based on the results of the sensitivity experiment with synthetic data, the following can be commented. Firstly, the three techniques based on the single isotope diffusion, perform similarly and of all the techniques tested, yield the highest precision with a $\sigma_{\bar{T}} \approx 0.5\,^{\circ}$C. Additionally, the estimated temperatures $\overline{T}_{\text{firn}}$ are within $1\sigma_{\bar{T}}$ of the forcing temperature T_{sur}, a result pointing to a good performance with respect to the accuracy of the temperature estimation. The precision of the differential diffusion techniques is inferior to single diffusion with $\sigma_{\bar{T}} \approx 1.2\,^{\circ}$C, with the subtraction technique being the least precise of all three differential diffusion approaches. A possible reason for this result may be the fact that the subtraction technique relies on the tuning of 8 optimization parameters as described in Sec. 4.1 and 4.2. On the contrary the correlation technique appears to be the most precise of the three techniques with precisions that are comparable of those achieved with the single diffusion techniques. All 10 experiments utilizing differential diffusion methods, yield an accuracy that lies within the $2\sigma_{\bar{T}}$ range ($1\sigma_{\bar{T}}$ range for 7

Table II: Ice core data sections and the corresponding drill site characteristic. Sources of data: (Steig et al. 2013)[1], (Oerter et al. 2004)[2]. Drill site characteristic sources: (Fegyveresi et al. 2011)[a], (Oerter et al. 2004, Veres et al. 2013)[b], (Watanabe et al. 2003)[c], (Lorius et al. 1979)[d], (Gkinis et al. 2014)[e], (Johnsen et al. 2000)[f], (Guillevic et al. 2013, Rasmussen et al. 2013)[g].

Site Name	Depth [m]	Age [kab2k]	Annual T [^{o}C]	A [myr^{-1}]	P [Atm]	Thinning	Meas.	Analysis	Δ [cm]
GRIP mid[f]	753 – 776	3.7	−31.6	0.23	0.65	0.71	δD, δ^{18}O	2130	2.5
GRIP late[f]	514 – 531	2.4	−31.6	0.23	0.65	0.79	δD, δ^{18}O	2130	2.5
WAIS 2005A[a,1]	260 – 290	1.1	−31.1	0.22	0.77	0.92	δ^{18}O	1102	5.0
EDML[b,2]	123 – 178	1.6	−44.6	0.08	0.67	0.93	δD, δ^{18}O	IRMS	5.0
NEEM[g]	174 – 194	0.8	−29.0	0.22	0.72	0.31	δD, δ^{18}O	2120	2.5
NGRIP[e]	174 – 194	0.9	−31.5	0.20	0.67	0.49	δ^{18}O	IRMS	2.5
Dome F[c]	302 – 307	9.6	−57.3	0.04	0.61	0.93	δD, δ^{18}O	CFA1102	0.5
Dome C[d]	308 – 318	9.9	−53.5	0.04	0.65	0.93	δD, δ^{18}O	IRMS	2.5
GRIP early[f]	1449 – 1466	9.4	−31.6	0.23	0.65	0.42	δD, δ^{18}O	2130	2.5
NEEM dis[g]	1380 – 1392	10.9	−29.0	0.22	0.72	0.31	δD, δ^{18}O	2120	5.0
NEEM CFA[g]	1382 – 1399	10.9	−29.0	0.22	0.72	0.31	δD, δ^{18}O	CFA1102	0.5
NGRIP I[e]	1300 – 1320	9.1	−31.5	0.18	0.67	0.55	δ^{18}O	IRMS	5.0
NGRIP II[e]	1300 – 1320	9.1	−31.5	0.18	0.67	0.55	δ^{18}O	IRMS	5.0

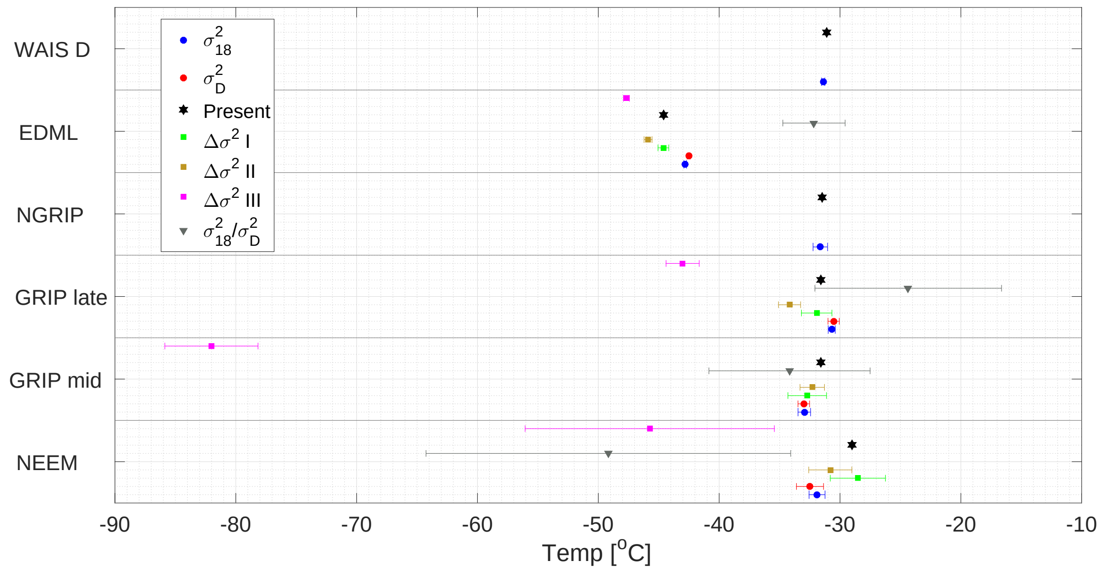

Figure 11: Reconstructed temperatures from the σ^2_{18} (blue circles), σ^2_{D} (red circles), $\Delta\sigma^2$ I (green squares), $\Delta\sigma^2$ II (brown squares), $\Delta\sigma^2$ III (magenta squares) and $\sigma^2_{18}/\sigma^2_{\mathrm{D}}$ (grey triangles) methods. The black stars represent the present annual mean temperatures at the sites.

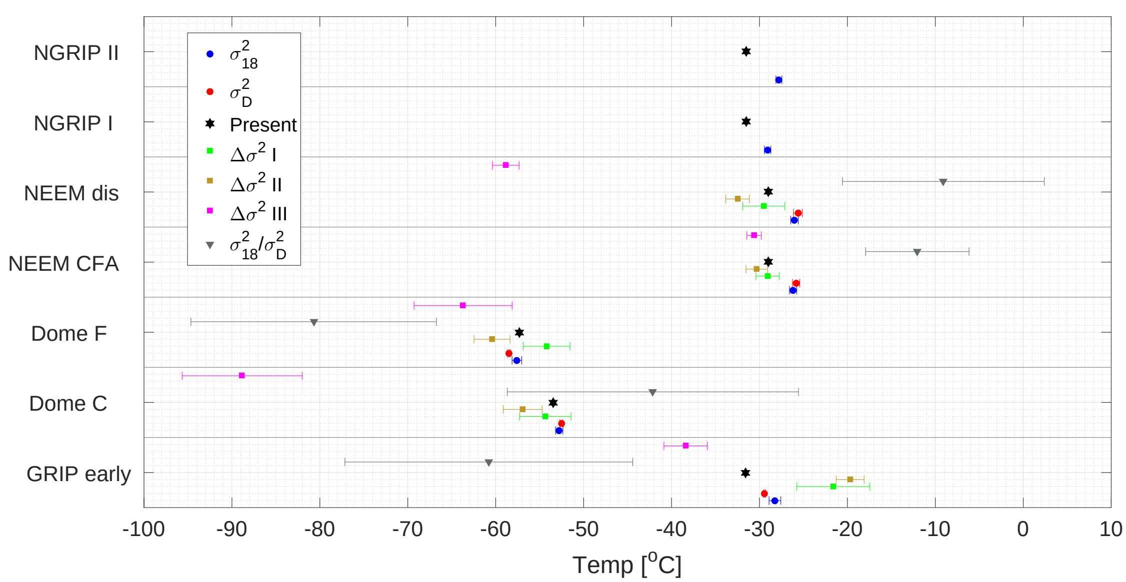

Figure 12: Reconstructed temperatures from the σ^2_{18} (blue circles), σ^2_{D} (red circles), $\Delta\sigma^2$ I (green squares), $\Delta\sigma^2$ II (brown squares), $\Delta\sigma^2$ III (magenta squares) and $\sigma^2_{18}/\sigma^2_{\mathrm{D}}$ (grey triangles) methods. The black stars represent the present annual mean temperatures at the sites.

Table III: Ice core results with the estimated firn diffusion lengths and their corresponding temperatures [$^{\circ}$C]. The units for the σ_{18} and the σ_{D} values are expressed in cm and the unit for $^{18}\Delta\sigma^2$ is expressed in cm^2.

Site Name	σ_{18}	σ_{D}	$^{18}\Delta\sigma^2$ I	$^{18}\Delta\sigma^2$ II	$^{18}\Delta\sigma^2$ III	$\sigma_{18}^2/\sigma_{\mathrm{D}}^2$
GRIP mid	7.83 ± 0.15 cm	7.20 ± 0.13 cm	9.4 ± 0.9 cm^2	9.6 ± 0.6 cm^2	0.2± 0.1 cm^2	1.18± 0.02
	-32.9± 0.5 °C	-33.0± 0.5 °C	-32.7 ± 1.6 °C	-32.3 ± 1.0 °C	-82.0 ± 3.9 °C	-34.2 ± 6.7 °C
GRIP late	8.52 ± 0.09 cm	7.92 ± 0.14 cm	9.9 ± 0.8 cm^2	8.6 ± 0.6 cm^2	4.8± 0.5 cm^2	1.16± 0.02
	-30.7 ± 0.3 °C	-30.5 ± 0.5 °C	-31.9 ± 1.3 °C	-34.2 ± 0.9 °C	-43.0 ± 1.4 °C	-24.4 ± 7.7 °C
WAIS 2005A	6.95 ± 0.04 cm	—	—	—	—	—
	-31.4 ± 0.1 °C	—	—	—	—	—
EDML	7.73 ± 0.04 cm	7.13 ± 0.04 cm	8.9 ± 0.3 cm^2	8.2 ± 0.2 cm^2	7.2± 0.1 cm^2	1.18± 0.01
	-42.8 ± 0.1 °C	-42.5 ± 0.1 °C	-44.6 ± 0.5 °C	-45.9 ± 0.3 °C	-47.7 ± 0.3 °C	-32.2 ± 2.6 °C
NEEM	7.97 ± 0.20 cm	7.20 ± 0.31 cm	11.7 ± 1.5 cm^2	10.2 ± 1.1 cm^2	4.5± 2.0 cm^2	1.23± 0.05
	-31.9 ± 0.7 °C	-32.5 ± 1.1 °C	-28.5 ± 2.3 °C	-30.8 ± 1.8 °C	-45.8 ± 10.3 °C	-49.2 ± 15.1 °C
NGRIP	8.65 ± 0.19 cm	—	—	—	—	—
	-31.6 ± 0.6 °C	—	—	—	—	—
Dome F	5.76 ± 0.15 cm	4.92 ± 0.04 cm	9.0 ± 1.8 cm^2	5.4 ± 0.8 cm^2	4.4± 1.9 cm^2	1.37± 0.08
	-57.6 ± 0.6 °C	-58.5 ± 0.2 °C	-54.2 ± 2.7 °C	-60.4 ± 2.1 °C	-63.7 ± 5.6 °C	-80.7 ± 14.0 °C
Dome C	6.97 ± 0.14 cm	6.34 ± 0.05 cm	8.4 ± 1.9 cm^2	6.7 ± 1.1 cm^2	0.43± 0.42 cm^2	1.21± 0.05
	-52.8 ± 0.4 °C	-52.5 ± 0.2 °C	-54.4 ± 2.9 °C	-56.9 ± 2.2 °C	-88.8 ± 6.8 °C	-42.1 ± 16.6 °C
GRIP early	9.32 ± 0.22 cm	8.25 ± 0.03 cm	18.7 ± 4.0 cm^2	20.4 ± 1.9 cm^2	6.6± 1.1 cm^2	1.27± 0.06
	-28.2 ± 0.7 °C	-29.4 ± 0.1 °C	-21.6 ± 4.2 °C	-19.7 ± 1.6 °C	-38.4 ± 2.5 °C	-60.8 ± 16.4 °C
NEEM dis	10.33 ± 0.16 cm	9.72 ± 0.19 cm	12.1 ± 1.8 cm^2	10.0 ± 0.8 cm^2	1.6± 0.2 cm^2	1.13± 0.02
	-26.0 ± 0.4 °C	-25.6 ± 0.5 °C	-29.5 ± 2.4 °C	-32.5 ± 1.3 °C	-58.9 ± 1.5 °C	-9.1 ± 11.5 °C
NEEM CFA	10.27 ± 0.15 cm	9.65 ± 0.15 cm	12.3 ± 1.0 cm^2	11.4 ± 0.9 cm^2	11.2± 0.6 cm^2	1.13± 0.01
	-26.2 ± 0.4 °C	-25.8 ± 0.4 °C	-29.1 ± 1.3 °C	-30.3 ± 1.2 °C	-30.6 ± 0.8 °C	-12.1 ± 5.9 °C
NGRIP I	9.68 ± 0.13 cm	—	—	—	—	—
	-29.1 ± 0.4 °C	—	—	—	—	—
NGRIP II	10.14 ± 0.12 cm	—	—	—	—	—
	-28.8 ± 0.3 °C	—	—	—	—	—

out of 10 experiments). We can conclude that experiments involving the estimation of the diffusion length ratio indicate that the latter are practically unusable due to very high uncertainties with $\sigma_{\bar{T}}$ averaging to a value of $\approx 12\,^{\circ}\mathrm{C}$ for all four experiments. A general trend that seems to be apparent for all the experiments, is that the results for the CD forcing yield slightly lower uncertainties when compared to those for the WH forcing, likely indicating a temperature and accumulation influence in the performance of all the reconstruction techniques.

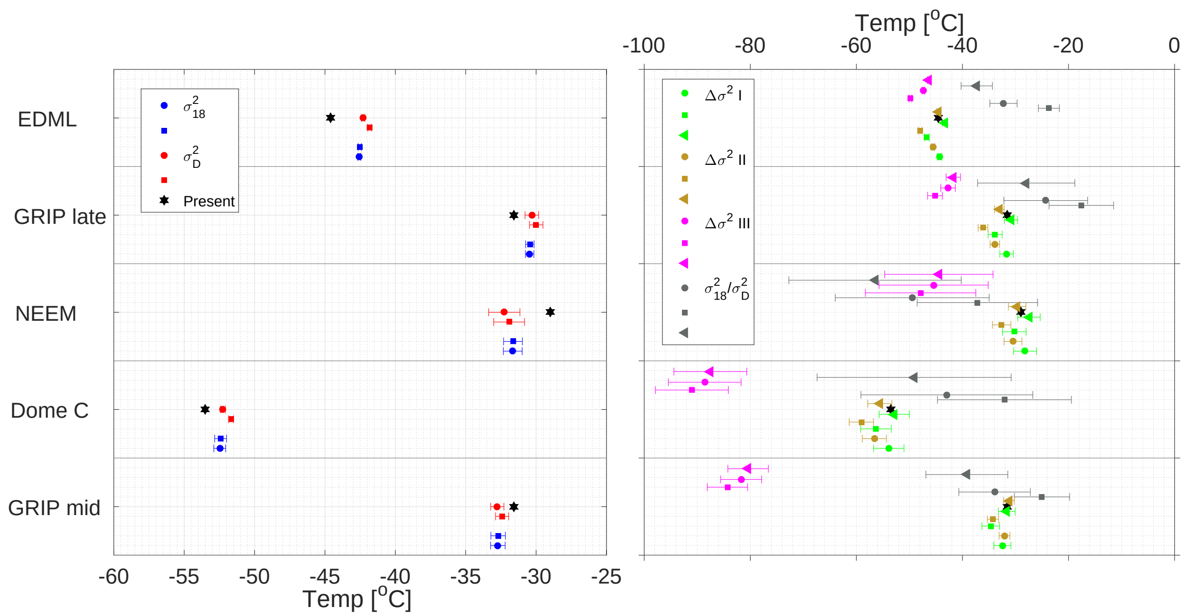

Figure 13: Temperature reconstructions based on different fractionation factor parametrizations. The left figure shows the single isotopologue methods and the right figure shows the dual isotope methods. The circles represent using the fractionation factors of Majoube (1970), Merlivat & Nief (1967), the squares represent Ellehoj et al. (2013) and the triangles represent Lamb et al. (2015), Majoube (1970).

6.2 Ice core data

The precision $\sigma_{\bar{T}}$ of each reconstruction technique has been quantified by averaging the standard deviations of the reconstructed temperatures (Table III). Hence, the precision represents the uncertainty of the estimated diffusion signal, and is not an indication of the accuracy of the absolute temperature estimate. In accordance with the results from the synthetic data test, the most precise reconstructions are obtained when using the single isotope diffusion methods. The single diffusion methods have a $\sigma_{\bar{T}}$ of $0.5\,^{\circ}$C, while the differential diffusion methods $^{18}\Delta\sigma^2$ I, II and III have a $\sigma_{\bar{T}}$ of $2.4\,^{\circ}$C, $1.5\,^{\circ}$C and $4.9\,^{\circ}$C, respectively. The correlation-based technique is hereby shown to be the least precise differential diffusion method. This differs from the result of the synthetic data, where the correlation-based technique was shown to be the most precise. Of the differential diffusion methods, the linear fit of the logarithmic ratio provides the most precise results, with a precision similar to that found from the synthetic data (Sec. 6.1). Of all the tested techniques, the diffusion length ratio method is the least precise with a $\sigma_{\bar{T}}$ of $11.8\,^{\circ}$C. A similar precision was found from the synthetic data.

It is not possible to quantify the accuracy of the methods when applied on ice core data, as the reconstructed temperatures represent the integrated firn column temperature. The reconstructed temperatures should therefore not necessarily be identical to present day annual temperatures. Instead, the root-mean-square deviation (RMSD) has been calculated in order to quantify the consistency between the reconstructed temperatures of any two methods (x and y):

$$\mathrm{RMSD} = \sqrt{\frac{\sum_{j=1}^{n} \left(x_j - y_j\right)^2}{n}}, \tag{6.1}$$

where j represents the drill site and n the total number of sites.

The temperature estimates originating from the σ_{18}^2 and σ_{D}^2 methods are found to have a RMSD of $0.7\,^{\circ}\mathrm{C}$. This shows that the σ_{18}^2 and σ_{D}^2 methods result in similar temperatures, which is consistent with the high accuracies found from the synthetic data test. In theory, ${}^{18}\Delta\sigma^2$ should yield even more accurate temperature estimates as it is independent of the systematic errors that can arise when correcting for ice and sampling diffusion. However, the RMSD between the temperature estimates of the ${}^{18}\Delta\sigma^2$ I and II techniques is found to be $3.8\,^{\circ}\mathrm{C}$. Even higher RMSDs is found between the temperature estimates of the ${}^{18}\Delta\sigma^2$ I and III, and the ${}^{18}\Delta\sigma^2$ II and III techniques. Here, the RMSDs are found to be $24.8\,^{\circ}\mathrm{C}$ and $23.8\,^{\circ}\mathrm{C}$, respectively. The large differences between the correlation-based and spectral-based temperature estimates are particularly pronounced for GRIP, NEEM (Fig. 11), Dome C and the discretely measured NEEM section (Fig. 12). In addition, it can be seen that the correlation-based method results in significantly different temperatures for the discretely and continuously measured NEEM section. A similar difference is not found from the spectral-based methods. Instead, these provide consistent temperatures independent of the processing scheme. Finally, a high RMSD ($24.5\,^{\circ}\mathrm{C}$) is also found when comparing the temperature estimates originating from the σ_{18}^2 and ${}^{18}\Delta\sigma^2$ III methods.

The generally poor performance of the correlation-based method on ice core data contradicts the high accuracy and precision of the synthetic reconstructions, and is most likely caused by an oversimplification of the relationship between $\delta\mathrm{D}$ and $\delta^{18}\mathrm{O}$. The generation of the synthetic data is based on the assumption that $\delta\mathrm{D} = 8\cdot\delta^{18}\mathrm{O} + 10‰$. However, this premise excludes the time dependent $\mathrm{D_{xs}}$ signal. The correlation-based method can therefore be used to accurately reconstruct synthetic temperatures, while the accuracy and precision is much lower for ice core data, as such data has been influenced by the $\mathrm{D_{xs}}$ signal. In addition, these temperature estimates have been shown to be dependent on the sampling process. The correlation-based method therefore yields uncertain estimates of the differential diffusion length.

The RMSDs between the temperature estimates of the σ_{18}^2 and ${}^{18}\Delta\sigma^2$ I methods, and the σ_{18}^2 and ${}^{18}\Delta\sigma^2$ II methods are found to be $3.9\,^{\circ}\mathrm{C}$ and $4.8\,^{\circ}\mathrm{C}$, respectively. This could therefore indicate that ${}^{18}\Delta\sigma^2$ I yields more accurate reconstructions than ${}^{18}\Delta\sigma^2$ II. However, ${}^{18}\Delta\sigma^2$ II has been shown to have the highest precision. It is therefore difficult to select the most accurate technique. One should therefore not have a preferred technique without utilizing both methods on longer ice core sections. Basically, the reconstructed temperatures could be similar when the temperatures have been averaged over a longer record.

Longer ice core sections can provide the foundation for evaluating how well other parameters are constrained. For instance, a wrong estimate of the thinning profile will scale the diffusion length estimates incorrectly and this will result in inaccurate temperature reconstructions. High resolution measurements of ice cores spanning the complete Holocene and last glacial maximum would help evaluate how well the accumulation rate history of past climate is reconstructed. For the NGRIP ice core, a complete temperature profile has been reconstructed using the σ^2_{18} method (Gkinis et al. 2014), but the profile had a temperature gradient of around $10\,^{\circ}\mathrm{C}$ between the HCO and present day. The high gradient was found to be caused by an error in the thinning profile. This pointed to a necessary adjustment of the ice flow's total thinning function indicating that the currently estimated accumulation rates were overestimated by 10% at 8ky b2k. This could be examined more thoroughly several places in Greenland and Antarctica by utilizing the single and differential diffusion techniques on ice cores spanning both the Holocene and last glacial maximum.

6.3 The fractionation factors

The temperature estimates resulting from the different fractionation factor parametrizations are shown in Fig. 13. For each method, the influence of the choice of parametrization on the reconstructed temperatures has been quantified by calculating the RMSD between temperature estimates of two parametrizations. Comparing the parametrizations of Ellehoj et al. (2013) to those of Majoube (1970) and Merlivat & Nief (1967), the RMSDs of reconstructions that are based on the single diffusion lengths σ^2_{18} and σ^2_{D} are $0.03^{\mathrm{o}}\mathrm{C}$ and $0.6^{\mathrm{o}}\mathrm{C}$. Thus, it is evident that the choice of fractionation factors has an insignificant effect on the results of the σ^2_{18} method and a small effect on the results of the σ^2_{D} method. The temperatures of the ${}^{18}\Delta\sigma^2$ techniques are more affected by the choice of parametrization, with the temperature estimates of the ${}^{18}\Delta\sigma^2$ I, II and III techniques having RMSDs of $2.3^{\mathrm{o}}\mathrm{C}$, $2.3^{\mathrm{o}}\mathrm{C}$ and $2.5^{\mathrm{o}}\mathrm{C}$, respectively. Comparing the parametrization of Lamb et al. (2015) to that of Merlivat & Nief (1967), the temperatures of the ${}^{18}\Delta\sigma^2$ I, II and III techniques have RMSDs of $0.9^{\mathrm{o}}\mathrm{C}$, $0.9^{\mathrm{o}}\mathrm{C}$ and $1.1^{\mathrm{o}}\mathrm{C}$, respectively. In general, smaller RMSDs are found when comparing with the temperature estimates based on the Lamb et al. (2015) parametrization. For instance, comparing the temperatures of the $\sigma^2_{18}/\sigma^2_{\mathrm{D}}$ technique based on Lamb et al. (2015) with those of Merlivat & Nief (1967), the $\sigma^2_{18}/\sigma^2_{\mathrm{D}}$ technique yields a RMSD of $5.4^{\mathrm{o}}\mathrm{C}$, while the RMSD is $9.7^{\mathrm{o}}\mathrm{C}$ when comparing the results based on the parametrizations of Ellehoj et al. (2013) with those of Majoube (1970) and Merlivat & Nief (1967). There are two reasons to why the RMSDs are smaller when comparing with the Lamb et al. (2015) parametrization: the parametrized α_{D} of Merlivat & Nief (1967) differs more with that of Ellehoj et al. (2013) than with that of Lamb et al. (2015), and the same α_{18} parametrization is used when comparing with Lamb et al. (2015).

The $\sigma_{18}^2/\sigma_{\mathrm{D}}^2$ method is significantly more influenced by the fractionation factors. The high RMSDs imply that even if the diffusion length ratio is estimated with high confidence, the method is still too sensitive to the choice of parameterization. This makes the method less suitable as a paleoclimatic thermometer.

7 Conclusions

This study assessed the performance of six different diffusion-based temperature reconstruction techniques. By applying the methods on synthetic data, it was demonstrated that each method could be used to accurately reconstruct unbiased temperatures. The precision of each technique was quantified by utilizing every variety of the diffusion-based temperature proxy on thirteen high resolution data sets from Greenland and Antarctica. The results showed that the single diffusion length methods yielded similar temperatures and that they are the most precise of all the presented reconstruction techniques. The most precise of the three differential diffusion length techniques was the linear fit of the logarithmic ratio. The most uncertain way of reconstructing past temperatures was by employing the diffusion length ratio method. The results from the correlation-based method were inconsistent to the results obtained through the spectral-based methods, and the method was considered to yield uncertain estimates of the differential diffusion length.

It was furthermore shown that the choice of fractionation factor parametrization only had a small impact on the results from the single diffusion length methods, while the influence was slightly higher for the differential diffusion length methods. The diffusion length ratio method was highly sensitive to the fractionation factor parametrization, and the method is not suitable as a paleoclimatic thermometer. From the combined analyses of the synthetic and ice core data, this study has demonstrated that methods based on the single isotope diffusion lengths result in the most accurate and precise estimates of past temperatures.

Authors' contributions

Author contributions

Acknowledgements

TEXT

Appendix A

Firn Diffusivity

We express the diffusivity as a function of firn density ρ and we use:

$$D(\rho) = \frac{m\,p\,D_{ai}}{R\,T\,\alpha_{\mathrm{i}}\,\tau}\left(\frac{1}{\rho} - \frac{1}{\rho_{\mathrm{ice}}}\right) \tag{A.1}$$

The terms used in Eq. (A.1) and the parametrization used for them are described below:

- m: molar weight (kg)
- p: saturation vapor pressure over ice (Pa). We use (Murphy & Koop 2006):

$$p = \exp\left(9.5504 - \frac{5723.265}{T} + 3.530\,\ln(T) - 0.0073\,T\right) \tag{A.2}$$

- D_{ai}: diffusivity of water vapor (for isotopologue i) in air ($\mathrm{m^2 s^{-1}}$). For the diffusivity of the abundant isotopologue water vapor D_{a} we use (Hall & Pruppacher 1970):

$$2.1 \cdot 10^{-5}\left(\frac{T}{T_o}\right)^{1.94}\left(\frac{P_o}{P}\right) \tag{A.3}$$

  with $P_{\mathrm{o}} = 1$ Atm, $T_{\mathrm{o}} = 273.15$ K and P, T the ambient pressure (Atm) and temperature (K). Additionally from Merlivat & Jouzel (1979) $D_{a^2\mathrm{H}} = 0.9755 D_{\mathrm{a}}$ and $D_{\mathrm{a}^{18}\mathrm{O}} = 0.9723 D_{\mathrm{a}}$ and from Barkan & Luz (2007) $D_{\mathrm{a}^{17}\mathrm{O}} = 0.98555 D_{\mathrm{a}}$.
- R: molar gas constant $R = 8.3144$ ($\mathrm{m^3 Pa K^{-1} mol^{-1}}$)
- T: Ambient temperature (K)
- α_{i}: Ice – Vapor fractionation factor. we use the formulations by Majoube (1970) and Merlivat & Nief (1967) for $\alpha^2_{\mathrm{s/v}}$ and $\alpha^{18}_{\mathrm{s/v}}$ respectively.

$$\alpha_{\mathrm{Ice/Vapor}}\left({}^2\mathrm{H}/{}^1\mathrm{H}\right) = 0.9098\exp(16288/T^2) \tag{A.4}$$

$$\alpha_{\mathrm{Ice/Vapor}}\left({}^{18}\mathrm{O}/{}^{16}\mathrm{O}\right) = 0.9722\exp(11.839/T) \tag{A.5}$$

$$\ln\left[\alpha_{\mathrm{Ice/Vapor}}\left({}^{17}\mathrm{O}/{}^{16}\mathrm{O}\right)\right] = 0.529\ln\left[\alpha_{\mathrm{Ice/Vapor}}\left({}^{18}\mathrm{O}/{}^{16}\mathrm{O}\right)\right] \tag{A.6}$$

- τ: The firn tortuosity. We use (Schwander et al. 1988):

$$\frac{1}{\tau} = 1 - b\cdot\left(\frac{\rho}{\rho_{\mathrm{ice}}}\right)^2 \quad \rho \le \frac{\rho_{\mathrm{ice}}}{\sqrt{b}},\ b = 1.3 \tag{A.7}$$

  Based on Eq. (A.7), $\tau \to \infty$ for $\rho > 804.3\,\mathrm{kgrm^{-3}}$

APPENDIX B

ICE DIFFUSIVITY

The solid ice diffusivity parametrization we use in this study is based on Ramseier (1967). In this section we provide the reader with parametrizations from other studies. We assume an Arrhenius type relationship for the ice diffusivity of the form:

$$D_{\text{ice}} = D_o \exp\left(-\frac{X}{T}\right) \; [\text{m}^2\text{s}^{-1}]. \tag{B.1}$$

In Eq. B.1, D_o is the pre-exponential factor in m^2s^{-1} and X is the Arrhenius coefficient where $X = Q/R$ with Q being the activation energy in kcalmol^{-1} and R the universal gas constant $(8.314\ \text{JK}^{-1}\text{mol}^{-1})$.

Results from four experimental studies are summarized in Table IV. Together with the pre-exponential factors and the activation energies, we also evaluate the four different expressions of ice diffusivities for the temperature of $T = 245\text{K}$.

When D_{ice} is known, a σ_{ice} calculation can be obtained by solving Eq. 2.5. Using the integrating factor $F = \exp\left(\int -2\dot{\varepsilon}_z\left(t\right)\text{d}t\right)$ we get:

$$\frac{\text{d}}{\text{d}t}\left(\sigma^2_{\text{ice}}\, e^{\int -2\dot{\varepsilon}_z(t)\text{d}t}\right) = 2D_{\text{ice}}\left(t\right)\, e^{\int -2\dot{\varepsilon}_z(t)\text{d}t} \tag{B.2}$$

This finally yields the ice diffusion length for a layer with age t' that has undergone ice flow thinning $S(t')$:

$$\sigma^2_{\text{ice}}\left(t'\right) = S\left(t'\right)^2 \int_0^{t'} 2D_{\text{ice}}\left(t\right) S\left(t\right)^{-2}\, \text{d}t \tag{B.3}$$

Table IV: Four experimental studies with their estimated activation energies (Q), the pre-exponential factors (D_0), the activation energies (X), and the corresponding ice diffusivities for the temperature of $T = 245\,\text{K}$ (D_{245}).

	D_o $[\text{m}^2\text{s}^{-1}]$	Q $[\text{kcalmol}^{-1}]$	X $[\text{K}^{-1}]$	D_{245} $[\text{m}^2\text{s}^{-1}]$
Ramseier (1967)	$9.2 \cdot 10^{-4}$	14.28	7186.5	$1.68 \cdot 10^{-16}$
Itagaki (1964)	0.014	14.97	7534.2	$6.18 \cdot 10^{-16}$
Blicks et al. (1966)	$2.5 \cdot 10^{-3}$	14.51	7302.4	$2.85 \cdot 10^{-16}$
Delibaltas et al. (1966)	$2.6 \cdot 10^{-3}$	15.66	7881.9	$2.83 \cdot 10^{-16}$

APPENDIX C

DISCRETE SAMPLING DIFFUSION

The sample diffusion length σ_{dis} is estimated by setting the transfer function of a Gaussian filter equal to a rectangular filter with width of the sample size Δ. The transfer function for the Gaussian filter in Eq. 2.3 is found by its Fourier transform:

$$\mathfrak{F}\left[\mathcal{G}\right] = \hat{\mathcal{G}} = e^{-\frac{k^2\sigma_{\mathrm{dis}}^2}{2}}. \tag{C.1}$$

A regular rectangle function is defined as:

$$\text{rect(t)} = \begin{cases} 1 & \text{for } -\frac{1}{2} < t < \frac{1}{2} \\ \frac{1}{2} & \text{for } t = |\frac{1}{2}| \\ 0 & \text{for } t > |\frac{1}{2}| \end{cases} \tag{C.2}$$

This can be transformed into a rectangular function ($\Pi(t)$) with width Δ and amplitude A:

$$\Pi(t) = A \cdot \text{rect}(t \cdot \Delta), \quad \text{for } -\frac{\Delta}{2} < t < \frac{\Delta}{2}. \tag{C.3}$$

Normalization yields an amplitude of $A = 1/\Delta$. The Fourier transformation of the rectangular pulse is written as:

$$\hat{\Pi}(f) = \int_{-\infty}^{\infty} \Pi(t) e^{-2\pi i f t} \mathrm{d}t = \int_{-\Delta/2}^{\Delta/2} \frac{1}{\Delta} e^{-2\pi i f_{\mathrm{Nq}} t} \mathrm{d}t, \tag{C.4}$$

where $f_{\mathrm{Nq}} = 1/(2\Delta)$ is the Nyquist frequency. Setting equations C.1 and C.4 equal to each other:

$$e^{-\frac{k^2\sigma_{dis}^2}{2}} = \int_{-\Delta/2}^{\Delta/2} \frac{1}{\Delta} e^{-2\pi i f_{nq} t} \mathrm{d}t, \tag{C.5}$$

where $k = 2\pi f_{\mathrm{Nq}}$. This results in the following solution for the discrete sampling diffusion length:

$$\sigma_{\mathrm{dis}}^2 = \frac{2\Delta^2}{\pi^2} \ln\left(\frac{\pi}{2}\right). \tag{C.6}$$

REFERENCES

Abramowitz, M. & Stegun, I. A. (1964), *Handbook of Mathematical Functions with Formulas, Graphs, and Mathematical Tables*, ninth dover printing, tenth gpo printing edn, Dover, New York.

Andersen, N. (1974), 'On The Calculation Of Filter Coefficients For Maximum Entropy Spectral Analysis', *Geophysics* **39**(1).

Baker, L., Franchi, I. A., Maynard, J., Wright, I. P. & Pillinger, C. T. (2002), 'A technique for the determination of o-18/o-16 and o-17/o-16 isotopic ratios in water from small liquid and solid samples', *Analytical Chemistry* **74**(7), 1665–1673.

Barkan, E. & Luz, B. (2005), 'High precision measurements of o-17/o-16 and o-18/o-16 ratios in h2o', *Rapid Communications In Mass Spectrometry* **19**(24), 3737–3742.

Barkan, E. & Luz, B. (2007), 'Diffusivity fractionations of (h2o)-o-16/(h2o)-o-17 and (h2o)-o-16/(h2o)-o-18 in air and their implications for isotope hydrology', *Rapid Communications In Mass Spectrometry* **21**(18), 2999–3005.

Begley, I. S. & Scrimgeour, C. M. (1997), 'High-precision δ^2H and δ^{18}O measurement for water and volatile organic compounds by continuous-flow pyrolysis isotope ratio mass spectrometry', *Analytical Chemistry* **69**(8), 1530–1535.

Bigeleisen, J., Perlman, M. L. & Prosser, H. C. (1952), 'Conversion of hydrogenic materials to hydrogen for isotopic analysis', *Analytical Chemistry* **24**(8), 1356–1357.

Blicks, H., Dengel, O. & Riehl, N. (1966), 'Diffusion von protonen (tritonen) in reinen und dotierten eis-einkristallen', *Physik Der Kondensiterten Materie* **4**(5), 375–381.

Brand, W. A., Geilmann, H., Crosson, E. R. & Rella, C. W. (2009), 'Cavity ring-down spectroscopy versus high-temperature conversion isotope ratio mass spectrometry; a case study on δ^2H and δ^{18}O of pure water samples and alcohol/water mixtures', *Rapid Communications in Mass Spectrometry* **23**(12), 1879–1884.

URL: *http://dx.doi.org/10.1002/rcm.4083*

Crosson, E. R. (2008), 'A cavity ring-down analyzer for measuring atmospheric levels of methane, carbon dioxide, and water vapor', *Applied Physics B-Lasers And Optics* **92**(3), 403–408.

Cuffey, K. M., Alley, R. B., Grootes, P. M., Bolzan, J. M. & Anandakrishnan, S. (1994), 'Calibration of the delta-o-18 isotopic paleothermometer for central greenland, using borehole temperatures', *Journal Of Glaciology* **40**(135), 341–349.

Dansgaard, W. (1954), 'The ^{18}O-abundance in fresh water', *Geochimica et Cosmochimica Acta* **Volume 6, Issues 56, pp: 241260**.

Dansgaard, W. (1964), 'Stable isotopes in precipitation', *Tellus B* **Vol: 16, Issue 4, pages: 436-468**.

Delibaltas, P., Dengel, O., Helmreich, D., Riehl, N. & Simon, H. (1966), 'Diffusion von ^{18}O in eis-einkristallen', *Physik Der Kondensiterten Materie* **5**(3), 166–170.

Ellehoj, M. D., Steen-Larsen, H. C., Johnsen, S. J. & Madsen, M. B. (2013), 'Ice-vapor equilibrium fractionation factor of hydrogen and oxygen isotopes: Experimental investigations and implications for stable water isotope studies', *Rapid Communications in Mass Spectrometry* **27, pp. 2149-2158**.

Emanuelsson, B. D., Baisden, W. T., Bertler, N. A. N., Keller, E. D. & Gkinis, V. (2015), 'High-resolution continuous-flow analysis setup for water isotopic measurement from ice cores using laser spectroscopy', *Atmos. Meas. Tech.* **8**(7), 2869–2883.

URL: *http://www.atmos-meas-tech.net/8/2869/2015/*

Epstein, S., Buchsbaum, R., LOWENSTAM, H. & Urey, H. (1951), 'Carbonate-water isotopic temperature scale', *Geological Society of America Bulletin* **62**(4), 417.

Fegyveresi, J. M., Alley, R. B., Spencer, M. K., Fitzpatrick, J. J., Steig, E. J., White, J. W. C., McConnell, J. R. & Taylor, K. C. (2011), 'Late-Holocene climate evolution at the WAIS Divide site, West Antarctica: bubble number-density estimates', *Journal of Glaciology* **57**(204).

Gehre, M., Hoefling, R., Kowski, P. & Strauch, G. (1996), 'Sample preparation device for quantitative hydrogen isotope analysis using chromium metal', *Analytical Chemistry* **68**(24), 4414–4417.

Gkinis, V., Popp, T. J., Blunier, T., Bigler, M., Schupbach, S., Kettner, E. & Johnsen, S. J. (2011), 'Water isotopic ratios from a continuously melted ice core sample', *Atmospheric Measurement Techniques* **4**(11), 2531–2542.

Gkinis, V., Simonsen, S. B., Buchardt, S. L., White, J. W. C. & Vinther, B. M. (2014), 'Water isotope diffusion rates from the NorthGRIP ice core for the last 16,000 years - glaciological and paleoclimatic implications', *Earth and Planetary Science Letters* **405**.

Guillevic, M., Bazin, L., Landais, A., Kindler, P., Orsi, A., Masson-Delmotte, V., Blunier, T., Buchardt, S. L., Capron, E., Leuenberger, M. ., Martinerie, P., Prie, F. & Vinther, B. M. (2013), 'Spatial gradients of temperature, accumulation and δ^{18}O-ice in Greenland over a series of Dansgaard-Oeschger events', *Climate of the Past* **9**, 10291051.

Hall, W. D. & Pruppacher, H. R. (1970), 'The survival of ice particles falling from cirrus clouds in subsaturated air', *Nature* **226**(1242).

Itagaki, K. (1964), 'Self-diffusion in single crystals of ice', *J. Phys. Soc. Jpn.* **19**(6), 1081–1081.

Johnsen, S., Clausen, H. B., Cuffey, K. M., Hoffmann, G., Schwander, J. & Creyts, T. (2000), 'Diffusion of stable isotopes in polar firn and ice: the isotope effect in firn diffusion', *Physics of Ice Core Records* .

Johnsen, S. J. (1977), 'Stable Isotope Homogenization of Polar Firn and Ice', *Isotopes and Impurities in Snow and Ice* pp. 210–219.

Johnsen, S. J., Dahl Jensen, D., Dansgaard, W. & Gundestrup, N. (1995), 'Greenland paleotemperatures derived from grip bore hole temperature and ice core isotope profiles', *Tellus Series B-Chemical And Physical Meteorology* **47**(5), 624–629.

Johnsen, S. J., DahlJensen, D., Gundestrup, N., Steffensen, J. P., Clausen, H. B., Miller, H., Masson-Delmotte, V., Sveinbjornsdottir, A. E. & White, J. (2001), 'Oxygen isotope and palaeotemperature records from six greenland ice-core stations: Camp century, dye-3, grip, gisp2, renland and northgrip', *Journal Of Quaternary Science* **16**(4), 299–307.

Jouzel, J., Alley, R. B., Cuffey, K. M., Dansgaard, W., Grootes, P., Hoffmann, G., Johnsen, S. J., Koster, R. D., Peel, D., Shuman, C. A., Stievenard, M., Stuiver, M. & White, J. (1997), 'Validity of the temperature reconstruction from water isotopes in ice cores', *Journal Of Geophysical Research-Oceans* **102**(C12), 26471–26487.

Jouzel, J. & Merlivat, L. (1984), 'Deuterium and oxygen 18 in precipitation: modeling of the isotopic effects during snow formation', *Journal of Geophysical Research-Atmospheres* **89**(D7), 11749 – 11759.

Kay, S. M. & Marple, S. L. (1981), 'Spectrum Analysis - A Modern Perspective', *Proceedings of the IEEE* **69**(11).

Lamb, K., Clouser, B., Bolot, M., Sarkozy, L., Ebert, V., Saathoff, H., Mhler, O. & Moyer, E. (2015), 'Laboratory measurements of HDO/H_2O isotopic fractionation during ice deposition in simulated cirrus clouds'. preprint.

Livingston, F. E., Whipple, G. C. & George, S. M. (1997), 'Diffusion of hdo into single-crystal (h2o)-o-16 ice multilayers: Comparison with (h2o)-o-18', *Journal of Physical Chemistry B* **101**(32), 6127–6131.

Lorius, C., Merlivat, L., Jouzel, J. & Pourchet, M. (1979), 'A 30,000-yr isotope climatic record from Antarctic ice', *Nature* **280**, 644 – 648.

Majoube, M. (1970), 'Fractionation factor of ^{18}O between water vapour and ice', *Nature* **226**(1242).

Meijer, H. A. J. & Li, W. J. (1998), 'The use of electrolysis for accurate delta o-17 and delta o-18 isotope measurements in water', *Isotopes In Environmental And Health Studies* **34**(4), 349–369.

members, N. (2004), 'High-resolution record of northern hemisphere climate extending into the last interglacial period', *Nature* **431**(7005), 147–151.

Merlivat, L. & Jouzel, J. (1979), 'Global Climatic Interpretation of the Deuterium-Oxygen 18 Relationship for Precipitation', *Journal of Geophysical Research* **84**(8).

Merlivat, L. & Nief, G. (1967), 'Fractionnement isotopique lors des changements detat solide-vapeur et liquide-vapeur de leau a des temperatures inferieures a 0 degrees c', *Tellus* **19**(1), 122–127.

Mook, J. (2000), *Environmental Isotopes in the Hydrological Cycle Principles and Applications*, International Atomic Energy Agency.

Murphy, D. M. & Koop, T. (2006), 'Review of the vapour pressures of ice and supercooled water for atmospheric applications', *Q.J.R. Meteorol. Soc.* **131, 15391565**.

Oerter, H., Graf, W., Meyer, H. & Wilhelms, F. (2004), 'The EPICA ice core Droning Maud Land: first results from stable-isotope measurements', *Ann. Glaciol.* **39**.

Press, W. H., Teukolsky, S. A., Vetterling, W. T. & Flannery, B. P. (2007), *Numerical Recipes: The Art of Scientific Computing*, Cambridge University Press.

Ramseier, R. O. (1967), 'Self-diffusion of tritium in natural and synthetic ice monocrystals', *Journal Of*

Applied Physics **38**(6), 2553–2556.

Rasmussen, S. O., Abbott, P. M., Blunier, T., Bourne, A., Brook, E., Buchardt, S. L., Buizert, C., Chappellaz, J., Clausen, H. B., Cook, E., Dahl-Jensen, D., Davies, S. M., Guillevic, M., Kipfstuhl, S., Laepple, T., Seierstad, I. K., Severinghaus, J., Steffensen, J. P., Stowasser, C., Svensson, A., Vallelonga, P., Vinther, B. M., Wilhelms, F. & Winstrup, M. (2013), 'A first chronology for the North Greenland Eemian Ice Drilling (NEEM) ice core', *Climate of the Past* **9**, 2713–2730.

Rasmussen, S. O., Bigler, M., Blockley, S. P., Blunier, T., Buchardt, S. L., Clausen, H. B., Cvijanovic, I., Dahl-Jensen, D., Johnsen, S. J., Fischer, H., Gkinis, V., Guillevic, M., Hoek, W. Z., Lowe, J. J., Pedro, J. B., Popp, T., Seierstad, I. K., Steffensen, J. P. P., Svensson, A. M., Vallelonga, P., Vinther, B. M., Walker, M. J., Wheatley, J. J. & Winstrup, M. (2014), 'A stratigraphic framework for abrupt climatic changes during the last glacial period based on three synchronized greenland ice-core records: refining and extending the intimate event stratigraphy', *Quaternary Science Reviews* **106**(0), 14–28.

Schwander, J., Stauffer, B. & Sigg, A. (1988), 'Air mixing in firn and the age of the air at pore close-off', *Annals of Glaciology* pp. pp. 141 –145.

Severinghaus, J. P. & Brook, E. J. (1999), 'Abrupt climate change at the end of the last glacial period inferred from trapped air in polar ice', *Science* **286**(5441), 930–934.

Severinghaus, J. P., Sowers, T., Brook, E. J., Alley, R. B. & Bender, M. L. (1998), 'Timing of abrupt climate change at the end of the younger dryas interval from thermally fractionated gases in polar ice', *Nature* **391**(6663), 141–146.

Simonsen, S. B., Johnsen, S. J., Popp, T. J., Vinther, B. M., Gkinis, V. & Steen-Larsen, H. C. (2011), 'Past surface temperatures at the NorthGRIP drill site from the difference in firn diffusion of water isotopes ', *Climate of the Past* **7**.

Steig, E. J., Ding, Q., White, J. W. C., Kttel, M., Rupper, S. B., Neumann, T. A., Neff, P. D., Gallant, A. J. E., Mayewski, P. A., Taylor, K. C., Hoffmann, G., Dixon, D. A., Schoenemann, S., M., M. B., Schneider, D. P., Fudge, T. J., Schauer, A. J., Teel, R. P., Vaughn, B., Burgener, L., Williams, J. & Korotkikh, E. (2013), 'Recent climate and ice-sheet change in West Antarctica compared to the past 2000 years', *Nature Geoscience* **6**.

Steig, E. J., Gkinis, V., Schauer, A. J., Schoenemann, S. W., Samek, K., Hoffnagle, J., Dennis, K. J. & Tan, S. M. (2014), 'Calibrated high-precision 17o-excess measurements using cavity ring-down spectroscopy with laser-current-tuned cavity resonance', *Atmos. Meas. Tech.* **7**(8), 2421–2435.
URL: *http://www.atmos-meas-tech.net/7/2421/2014/*

van der Wel, G., Fischer, H., Oerter, H., Meyer, H. & Meijer, H. A. J. (2015), 'Estimation and calibration of the water isotope differential diffusion length in ice core records', *The Cryosphere* **9**(4), 1601–1616.

URL: *http://www.the-cryosphere.net/9/1601/2015/*

Vaughn, B. H., White, J. W. C., Delmotte, M., Trolier, M., Cattani, O. & Stievenard, M. (1998), 'An automated system for hydrogen isotope analysis of water', *Chemical Geology* **152**(3-4), 309–319.

Veres, D., Bazin, L., Landais, A., Kele, H. T. M., Lemieux-Dudon, B. B., Parrenin, F., Martinerie, P., Blayo, E., Blunier, T., Capron, E., Chappellaz, J., Rasmussen, S. O., Severi, M., Svensson, A., Vinther, B. & Wolff, E. W. (2013), 'The Antarctic ice core chronology (AICC2012): an optimized multi-parameter and multi-site dating approach for the last 120 thousand years', *Climate of the Past* **9**.

Vinther, B. M., Clausen, H. B., Johnsen, S. J., Rasmussen, S. O., Andersen, K. K., Buchardt, S. L., Dahl-Jensen, D., Seierstad, I. K., Siggaard-Andersen, M. L., Steffensen, J. P., Svensson, A., Olsen, J. & Heinemeier, J. (2006), 'A synchronized dating of three greenland ice cores throughout the holocene', *Journal Of Geophysical Research-Atmospheres* **111**(D13), D13102.

Watanabe, O., Shoji, H., Satow, K and, M. H., Fujii, Y., Narita, H. & S., A. (2003), 'Dating of the Dome Fuji, Antarctica deep ice core', *Mem. Natl Inst. Polar Res., Spec. Issue* **57**, 25–37.